nature neuroscience

Meigo governs dendrite targeting specificity by modulating Ephrin level and *N*-glycosylation

Sayaka U Sekine[1], Shuka Haraguchi[1], Kinhong Chao[1], Tomoko Kato[1], Liqun Luo[2], Masayuki Miura[1,3] & Takahiro Chihara[1,4]

Neural circuit assembly requires precise dendrite and axon targeting. We identified an evolutionarily conserved endoplasmic reticulum (ER) protein, Meigo, from a mosaic genetic screen in *Drosophila melanogaster*. Meigo was cell-autonomously required in olfactory receptor neurons and projection neurons to target their axons and dendrites to the lateral antennal lobe and to refine projection neuron dendrites into individual glomeruli. Loss of Meigo induced an unfolded protein response and reduced the amount of neuronal cell surface proteins, including Ephrin. Ephrin overexpression specifically suppressed the projection neuron dendrite refinement defect present in *meigo* mutant flies, and *ephrin* knockdown caused a similar projection neuron dendrite refinement defect. Meigo positively regulated the level of Ephrin *N*-glycosylation, which was required for its optimal function *in vivo*. Thus, Meigo, an ER-resident protein, governs neuronal targeting specificity by regulating ER folding capacity and protein *N*-glycosylation. Furthermore, Ephrin appears to be an important substrate that mediates Meigo's function in refinement of glomerular targeting.

During neural development, the axon and dendrites of each neuron are confronted with a difficult task: finding the appropriate synaptic partners among a sea of inappropriate ones to form a functional neural circuit. In the past two decades, the molecular mechanisms of axon targeting have been intensively studied. Although axon guidance and target selection are classically believed to dominate neural circuit formation, active dendrite processes are also indispensable for proper patterning. For example, vertebrate retinal ganglion cells target their dendrites to specific laminar layers to make synaptic connections with bipolar and amacrine cells[1]. In addition, oriented dendrite patterning of mouse motor neurons is actively regulated by the expression of the ETS transcription factor *Pea3*, which is itself induced by sensory stimuli[2]. Relatively little is known in general, however, about the molecular mechanisms of dendrite targeting.

The *Drosophila* olfactory system provides an excellent opportunity to examine the molecular mechanisms that underlie both dendrite and axon targeting[3,4]. In the adult antennal lobe, axons of ~50 classes of olfactory receptor neurons (ORNs) and dendrites of ~50 classes of second-order projection neurons typically target one of ~50 glomeruli, forming one-to-one precise connections (**Fig. 1a**). The target glomerulus of each projection neuron dendrite is pre-specified by birth order and the intrinsic activity of transcription factors[4,5]. Projection neuron dendrite targeting occurs before invasion of the antennal lobe by presynaptic ORN axons, suggesting an independent regulation of both processes[6]. During the initial coarse targeting, developing projection neuron dendrites express a gradient of Semaphorin-1a (Sema-1a), which acts as a receptor for potential ligands Sema-2a and Sema-2b, along the dorsolateral-to-ventromedial axis in the antennal lobe[7,8]. After the coarse targeting, synaptic partner matching and refinement of each class of projection neuron dendrites are carried out by the activity of various cell-surface transmembrane molecules, such as DN-Cadherin, Capricious, Dscam and the Teneurins[9–12]. Thus, previous studies have revealed the coordinated interconnection of multiple cell surface molecules.

As the vast majority of proteins used for the target recognition in dendrites are secretory and cell surface proteins, their folding and initial glycosylation occur in the ER. To assist the maturation of proteins, the lumen of the ER provides access to numerous enzymes and chaperones. In addition, chaperones such as calreticulin and calnexin provide a quality control mechanism that ensures only correctly folded proteins are released by transient binding through the *N*-glycan that is attached to newly synthesized protein. Thus, the capacity to produce the mature proteins at the ER (hereafter referred to as ER folding capacity) greatly depends on the cell condition, particularly the expression level and combination of various enzymes, chaperones and components of the *N*-glycosylation machinery[13,14]. If the translation of secretory proteins exceeds the ER folding capacity, the overload of unfolded protein at the ER induces an evolutionarily conserved signal transduction mechanism, the so called unfolded protein response (UPR)[15]. As a consequence of the UPR, general translation is attenuated, the expression of enzymes, chaperones and *N*-glycosylation-related genes are upregulated, and the ER-associated degradation system to eliminate the unfolded proteins is activated[16]. Although the UPR is thought to act especially in pathological conditions, it is also essential for normal development[17,18]. However, it is still unclear how ER folding capacity and the UPR are managed in developing neurons, which require both a large amount and variety of functional transmembrane and secreted proteins.

[1]Department of Genetics, Graduate School of Pharmaceutical Sciences, University of Tokyo, Tokyo, Japan. [2]Howard Hughes Medical Institute and Department of Biology, Stanford University, Stanford, California, USA. [3]Core Research for Evolutional Science and Technology, Japan Science and Technology Agency, Tokyo, Japan. [4]Precursory Research for Embryonic Science and Technology, Japan Science and Technology Agency, Tokyo, Japan. Correspondence should be addressed to T.C. (tchihara@mol.f.u-tokyo.ac.jp).

Received 15 February; accepted 1 April; published online 28 April 2013; doi:10.1038/nn.3389

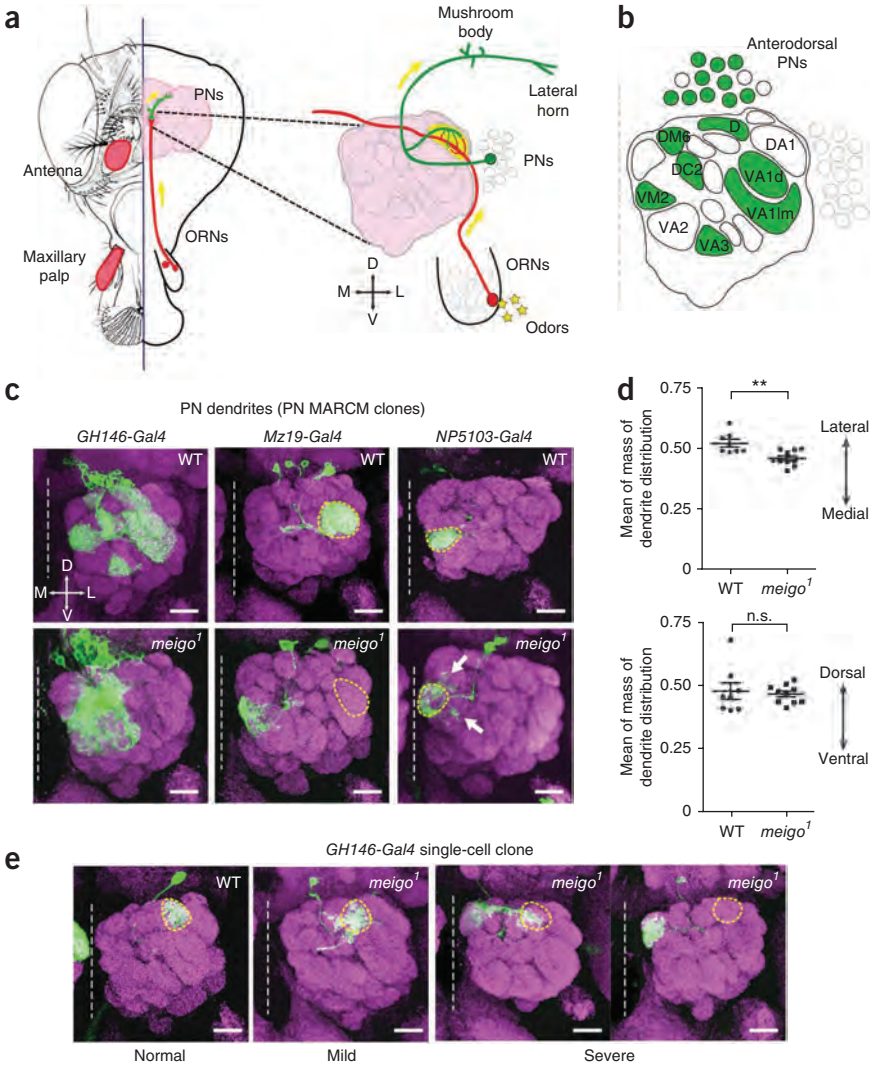

Figure 1 *meigo*^{1} projection neuron dendrites are defective in mediolateral targeting and glomerular refinement. (**a**) Schematic of the *Drosophila* olfactory system. ORNs (red) and projection neurons (PNs, green) target their axons and dendrites to genetically pre-specified target glomeruli (yellow) to generate one-to-one neural connections in the antennal lobe. Arrows indicate the flow of olfactory information. (**b**) Schematic of the MARCM projection neuron neuroblast clones of anterodorsal lineage labeled by *GH146-Gal4*. The target glomeruli of anterior surface of the antennal lobe are colored in green. The name of each glomerulus is also indicated. (**c**) Projection neurons derived from wild-type (WT) or *meigo*^{1} anterodorsal neuroblast MARCM clones were labeled by *GH146-Gal4*, *Mz19-Gal4* or *NP5103-Gal4*. Dendrites of *meigo*^{1} projection neurons accumulated on the medial side of the antennal lobe. Yellow dotted lines indicate the target glomerulus of wild-type projection neurons. The white arrows indicate the spillover of dendrites. Green indicates mCD8-GFP–labeled projection neurons and magenta represents the presynaptic marker Brp. The white dotted lines indicate the midline. Scale bars represent 20 μm. (**d**) Quantification of the relative intensity of dendrite fluorescence of anterodorsal neuroblast clones (labeled by *GH146-Gal4)* along the mediolateral or dorsoventral axis of the antennal lobe. A significant medial shift of the dendrites was revealed, but no significant difference was observed dorsoventrally (wild type (n = 8) versus *meigo*^{1} (n = 10 individual MARCM clones): mediolateral, $^{**}P < 0.025$; dorsoventral, not significant (n.s., $P > 0.05$)). Error bars indicate s.e.m. (**e**) Dendrite targeting of single-cell MARCM clones of the DL1 class of wild-type or *meigo*^{1} projection neurons. The yellow dotted lines indicate the DL1 glomerulus. Three examples of *meigo*^{1} projection neuron single-cell clones are shown. Normal: dendrites properly targeted and were restricted to the DL1 glomerulus. Mild: dendrites targeted around the DL1 glomerulus with spillover to neighboring (mostly medial) glomeruli. Severe: most dendrite branches mistargeted medial to DL1. Data are presented as in **c**.

We isolated and characterized Meigo, an evolutionarily conserved protein that is required for the precise targeting of projection neuron dendrites and ORN axons in the *Drosophila* olfactory system. Meigo is the *Drosophila* homolog of SLC35B1, an ER-resident protein that belongs to the nucleotide sugar transporter family[19]. Loss of Meigo induced UPR in projection neuron dendrites, which led to a decrease in the amount of cell surface proteins, including Ephrin. Biochemical analyses revealed that Meigo promoted the proper *N*-glycosylation and cell surface localization of Ephrin, which, in part, mediated Meigo's *in vivo* function. We propose that Meigo enhances the ER folding capacity by contributing to the *N*-glycosylation machinery, ensuring the production of multiple cell surface proteins that are required for dendrite and axon targeting.

RESULTS

meigo is required in projection neurons for dendrite targeting

To identify genes that regulate neuronal targeting specificity, we performed a mosaic analysis with a repressive cell marker (MARCM)-based genetic mosaic screen in projection neurons[20] and isolated a dendrite targeting mutant, *meigo*^{1} (*medial glomeruli*, 'lost child' in Japanese). In MARCM anterodorsal neuroblast clones homozygous for *meigo*^{1} in an otherwise heterozygous background, the *meigo*^{1} projection neurons labeled with the projection neuron driver *GH146-Gal4* exhibited improper medial shift of dendrite targeting in the antennal lobe (**Fig. 1b**,**c**). Using the *Mz19-Gal4* driver, which labels a small subset of projection neurons, dendrites that normally target the laterally located glomeruli (VA1d and DC3) also shifted medially (**Fig. 1c**). In contrast, projection neurons labeled by the *NP5103-Gal4* driver[21], which normally target the medial glomerulus VM2, still targeted properly, with a glomerular spillover (46%, n = 13; **Fig. 1c**). Quantification of these dendrite distributions revealed that, although lateral *meigo*^{1} dendrites were significantly shifted medially ($P < 0.025$), they retained their normal position along the orthogonal dorsoventral axis (**Fig. 1d**). This was also observed in neuroblast clones of the lateral lineage (**Supplementary Fig. 1a**,**b**). This phenotype was already evident at early pupal stages (16 h after puparium formation), when initial projection neuron targeting occurs (**Supplementary Fig. 1c**), suggesting that the initial dendrite targeting to the proto-antennal lobe is defective in *meigo*^{1} projection neurons.

To analyze projection neuron dendrite targeting with higher resolution, we generated *meigo*^{1} projection neuron single-cell clones whose dendrites, in wild-type neurons, target the DL1 glomerulus. As with *meigo*^{1} neuroblast clones, the majority of *meigo*^{1} DL1 projection neuron

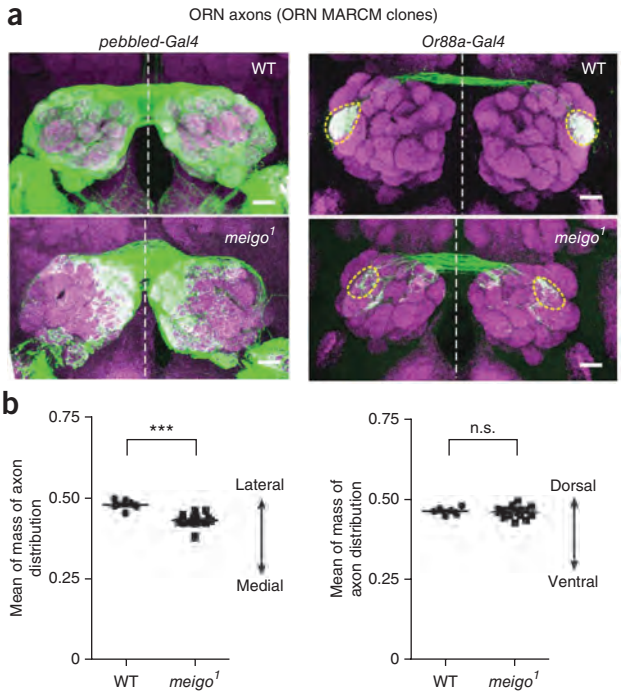

Figure 2 Targeting defects of *meigo*^{1} ORN axons. (**a**) Wild-type and *meigo*^{1} MARCM ORN clones induced by *ey-FLP* and visualized by *pebbled-Gal4* or *Or88a-Gal4*. ORN axons were also misdirected medially in *meigo*^{1} clones. Green indicates mCD8-GFP–labeled ORNs. The yellow dotted lines indicate the target glomeruli of wild-type ORNs. Magenta represents the presynaptic marker Brp. The white dotted lines indicate the midline. Scale bars represent 20 μm. (**b**) Quantification of the relative intensity of axon fluorescence of MARCM clones (labeled by *pebbled-Gal4*) along the mediolateral or dorsoventral axis of the antennal lobe. A significant medial shift of the axons was revealed, but no significant difference was observed dorsoventrally (wild type ($n = 6$) versus *meigo*^{1} ($n = 17$): mediolateral, $^{***}P < 0.001$; dorsoventral, not significant (n.s., $P > 0.05$)). Error bars indicate s.e.m.

single-cell clones had marked defects in dendrites targeting along the mediolateral axis. Often, dendrites of *meigo*^{1} single-cell clones failed to refine into the DL1 glomerulus and innervated multiple glomeruli located medially to DL1 (**Fig. 1e**). We classified this phenotypic severity into three groups and found a highly penetrant medial shift of *meigo*^{1} DL1 projection neuron dendrites (normal, 0%; mild, 81%; severe, 19%; $n = 37$ individual single-cell clones). These mutant phenotypes suggest that *meigo* has two functions: dendrite targeting selectively along the mediolateral axis of the antennal lobe and refinement of dendrites of individual projection neurons into a single glomerulus.

meigo is independently required in ORNs for axon targeting

To examine the effect of the *meigo*^{1} on ORN axon targeting, we used *eyeless-FLP* MARCM to generate mutant clones in the sensory organs[22] (including ORNs), but not in the brain, and concomitantly labeled all or one class of mutant ORNs using *pebbled-Gal4* (ref. 23) or *Or88a-Gal4* (ref. 24), respectively. Compared with wild-type ORN clones, axons of *meigo*^{1} ORN clones strongly innervated the medial antennal lobe (**Fig. 2a**). The quantification of axon innervation in the antennal lobe revealed that *meigo*^{1} ORN axons also exhibited a significant medial shift in their glomerular targeting ($P < 0.001$), similar to mutant projection neuron dendrites (**Fig. 2b**).

Together with our projection neuron analysis (**Fig. 1**), these data indicate that *meigo* is independently required in projection neurons and ORNs for lateral targeting of their dendrites and axons, respectively. This suggests that projection neurons and ORNs utilize shared positional signal(s) along the mediolateral axis of the antennal lobe to reach target glomeruli. The *meigo*^{1} mutation likely disrupts the recognition of this putative mediolateral positional signal(s) in the antennal lobe.

meigo encodes a highly conserved ER protein

We mapped *meigo*^{1} to a missense mutation in *CG5802*, encoding an evolutionarily conserved protein, at a residue conserved from fly to human (67.5% similar to yeast *hut1*, 81.2% to *C. elegans hut1*, 81.0% to mouse *UGTrel1* (also known as *Slc35b1*) and 80.7% to human *UGTrel1* (also known as *SLC35B1*); **Supplementary Fig. 2a**). To confirm that this is the causative mutation for the *meigo* phenotype, we created a deletion that removed the N-terminal half of the predicted CG5802 protein (*CG5802*^{del}; **Supplementary Fig. 2a**). We found that *CG5802*^{del} projection neuron clones exhibited the same dendrite mistargeting as *meigo*^{1} projection neuron clones (**Supplementary Fig. 2b**). In addition, MARCM expression of the *CG5802* cDNA rescued the phenotype of *meigo*^{1} projection neuron neuroblast and single-cell clones (**Supplementary Fig. 2c**). These results indicate that *meigo* corresponds to *CG5802*. Furthermore, as *GH146-Gal4* is only expressed in postmitotic projection neurons, these results suggest that Meigo is required both cell autonomously and postmitotically in projection neuron dendrite targeting. The phenotype of *meigo*^{1} ORN clones was also rescued by the *pebbled-GAL4*–mediated transgenic expression of *CG5802* and *meigo* cDNA in those clones (**Supplementary Fig. 2c**).

meigo encodes a transmembrane protein with a KKXX ER retention motif near the C terminus that is conserved from yeast to human (**Fig. 3a** and **Supplementary Fig. 2d**). Consistently, both endogenous (**Fig. 3b**) and transiently overexpressed (**Supplementary Fig. 3a**) Meigo in *Drosophila* S2 cells decorated an ER-like membranous structure. To confirm the ER localization of Meigo, we used OptiPrep density centrifugation[25] to isolate membrane fractions of the ER and Golgi apparatus. Meigo was predominantly accumulated in the fractions that contained Hsc3, an ER-resident chaperone (also known as GRP78/BiP; **Fig. 3c**). Lava Lamp (Lva)[26], a marker of Golgi apparatus was found in fractions that are slightly overlapped with, but were clearly different from, those of Meigo (**Fig. 3c**). These immunohistochemical and biochemical data indicate that Meigo is mainly localized at the ER.

Meigo is a unique nucleotide sugar transporter

Meigo is a predicted ortholog of human *UGTrel1* (ref. 23), the nucleotide sugar transporter (NST) that transports nucleotide sugars from the cytoplasm to the lumens of the ER[27], an essential step for proper protein glycosylation. To test whether defects in NST can generally cause projection neuron mistargeting, we generated MARCM projection neuron clones for the other NST mutants (**Fig. 3d**). *fringe connection* (*frc*) and *slalom* (*sll*) encode UDP-sugar and 3′-phosphate 5′-phosphosulfate transporters, respectively[28–30]. Notably, *frc*^{RY34} or *sll*^{24533} projection neuron clones did not exhibit any targeting defects (**Supplementary Fig. 3b**). In addition, MARCM overexpression of *frc*, *sll* or *ER GDP-fucose transporter* (*Efr*)[31] in *meigo*^{1} projection neuron clones could not suppress the dendrite targeting defect (**Fig. 3e**), indicating that Meigo cannot be substituted for by other NSTs.

To examine the importance of glycosylation for projection neuron dendrite targeting, we examined mutations in several glycosyltransferases. We found that mutant MARCM clones of glycosyltransferases necessary for the mucin-type *O*-glycan[32], sialylated carbohydrates[33], heparan sulfate proteoglycans and chondroitin sulfate proteoglycans[34–36] did not

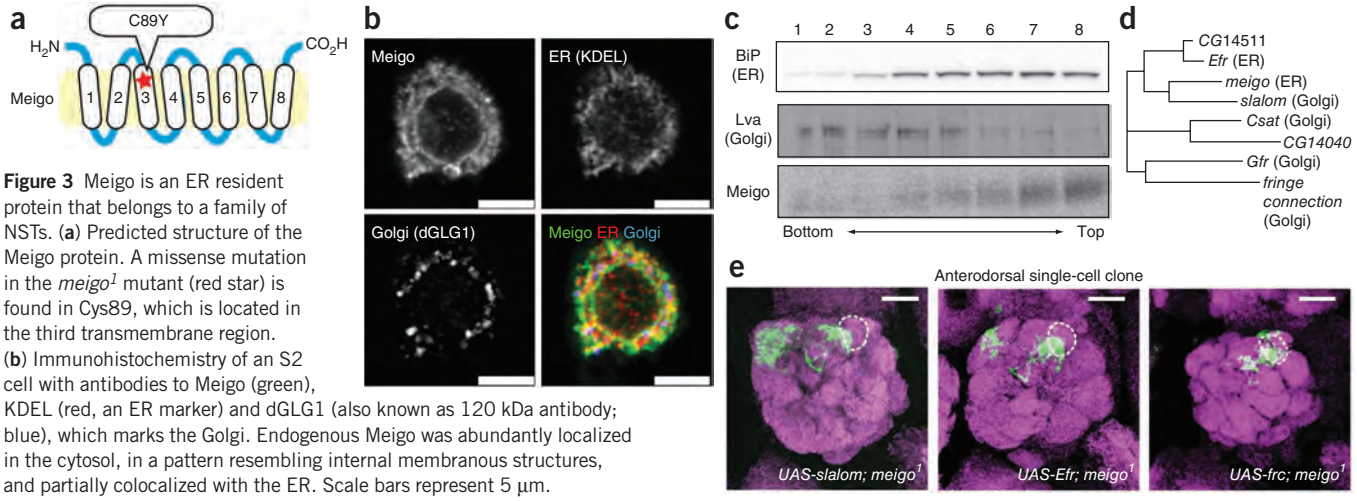

Figure 3 Meigo is an ER resident protein that belongs to a family of NSTs. (**a**) Predicted structure of the Meigo protein. A missense mutation in the *meigo*^{1} mutant (red star) is found in Cys89, which is located in the third transmembrane region. (**b**) Immunohistochemistry of an S2 cell with antibodies to Meigo (green), KDEL (red, an ER marker) and dGLG1 (also known as 120 kDa antibody; blue), which marks the Golgi. Endogenous Meigo was abundantly localized in the cytosol, in a pattern resembling internal membranous structures, and partially colocalized with the ER. Scale bars represent 5 μm. (**c**) Immunoblots of fractions from a membrane density gradient revealed that a significant portion of Meigo was present in fractions enriched with the ER membrane. The top and bottom of the gradient are indicated below the panels. The full-length blots are presented in **Supplementary Figure 7**. (**d**) A phylogenetic tree of *Drosophila* genes predicted to have NST activity. The subcellular localization is shown in parentheses. (**e**) Overexpression of the other NSTs, *slalom*, *Efr* or *frc*, did not suppress the dendrite mistargeting of *meigo*^{1} single-cell clones, suggesting that these NSTs cannot substitute for Meigo in projection neuron dendrite targeting. Green indicates projection neuron MARCM clones and magenta indicates Brp staining. Scale bars represent 20 μm.

exhibit dendrite mistargeting along the mediolateral axis like *meigo*^{1} (**Supplementary Table 1**). On the other hand, the mutant MARCM clones for *fused lobes*[37] encoding an *N*-acetylglucosaminidase, which is required for the maturation of *N*-glycans, showed a cell lethal phenotype. This result suggests that *N*-glycans are essential for the cell viability of projection neurons, which makes it difficult to investigate their role in dendrite targeting. Taken together, the dendrite phenotype of *meigo*^{1} projection neurons could not be explained by the general impairment of NST activity and is not likely a result of the defect in the synthesis of mucin-type *O*-glycan, sialylated carbohydrates, heparan sulfate proteoglycans and chondroitin sulfate proteoglycans. Thus, Meigo appears to have a unique function in projection neuron dendrite targeting among NSTs.

meigo knockdown induces UPR

We then asked what occurs in cells that lack Meigo. *hut1*, the yeast homolog of *meigo*, is required for ER stress resistance[38]. In *C. elegans*,

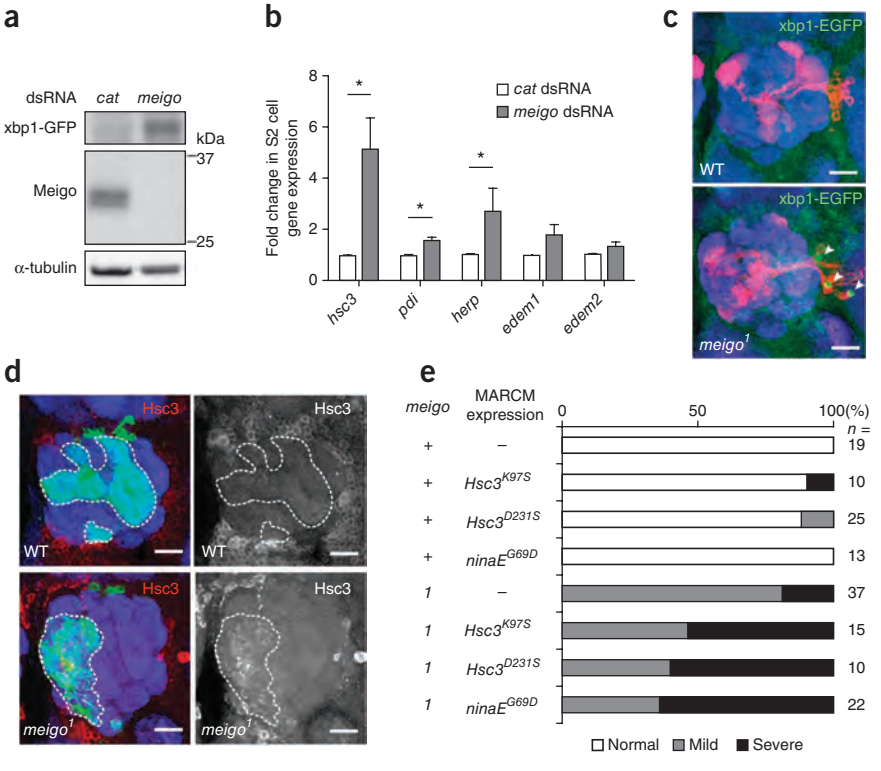

Figure 4 Meigo mediates ER homeostasis in projection neurons. (**a**) Western blot analysis detected the unconventional splicing of *xbp1-EGFP* that was induced by ER stress in *meigo*-knockdown S2 cells. *cat* dsRNA was used as a negative control. Antibody to Meigo detects a 32-kDa band on a western blot, which corresponds to the predicted molecular weight of Meigo. Antibody to α-tubulin loading controls are shown below. The full-length blots are presented in **Supplementary Figure 7**. (**b**) Measurement of mRNA levels of unfolded protein response target genes (*hsc3*, *pdi*, *herp*, *edem1* and *edem2*) by quantitative reverse transcription (RT)-PCR of S2 cell lysates treated with *cat* dsRNA or *meigo* dsRNA. Meigo depletion induced upregulation of UPR target gene expression ($n = 4$; $^{*}P < 0.05$ for *hsc3, pdi* and *herp*). Error bars indicate s.e.m. (**c**) MARCM expression of *xbp1-EGFP* in wild-type or *meigo*^{1} neuroblast clone of lateral lineage. The Xbp1-EGFP accumulated in the nuclei of *meigo*^{1}, but not wild-type, projection neurons. Red indicates mCD8-RFP–labeled projection neurons, and blue represents the presynaptic marker Brp. Scale bars represent 20 μm. (**d**) Hsc3 staining (red) in wild-type or *meigo*^{1} neuroblast clones. The enhanced Hsc3 signals in the medially shifted dendrites were observed only in *meigo*^{1} neuroblast clones. Green marks mCD8-GFP–labeled projection neurons. Blue represents the presynaptic marker Brp. Scale bars represent 20 μm. (**e**) Quantification of the severity of the phenotype of *meigo*^{1} single-cell clones overexpressing molecules that induce ER stress. Expression of *Hsc3*^{K97S}, *Hsc3*^{D231S} or *ninaE*^{G69D} in wild-type (+) single-cell clones had either a weak effect or no effect; however, expression in *meigo*^{1} (*1*) single-cell clones enhanced the targeting defect, suggesting that mutation of *meigo* enhances sensitivity to the ER stress.

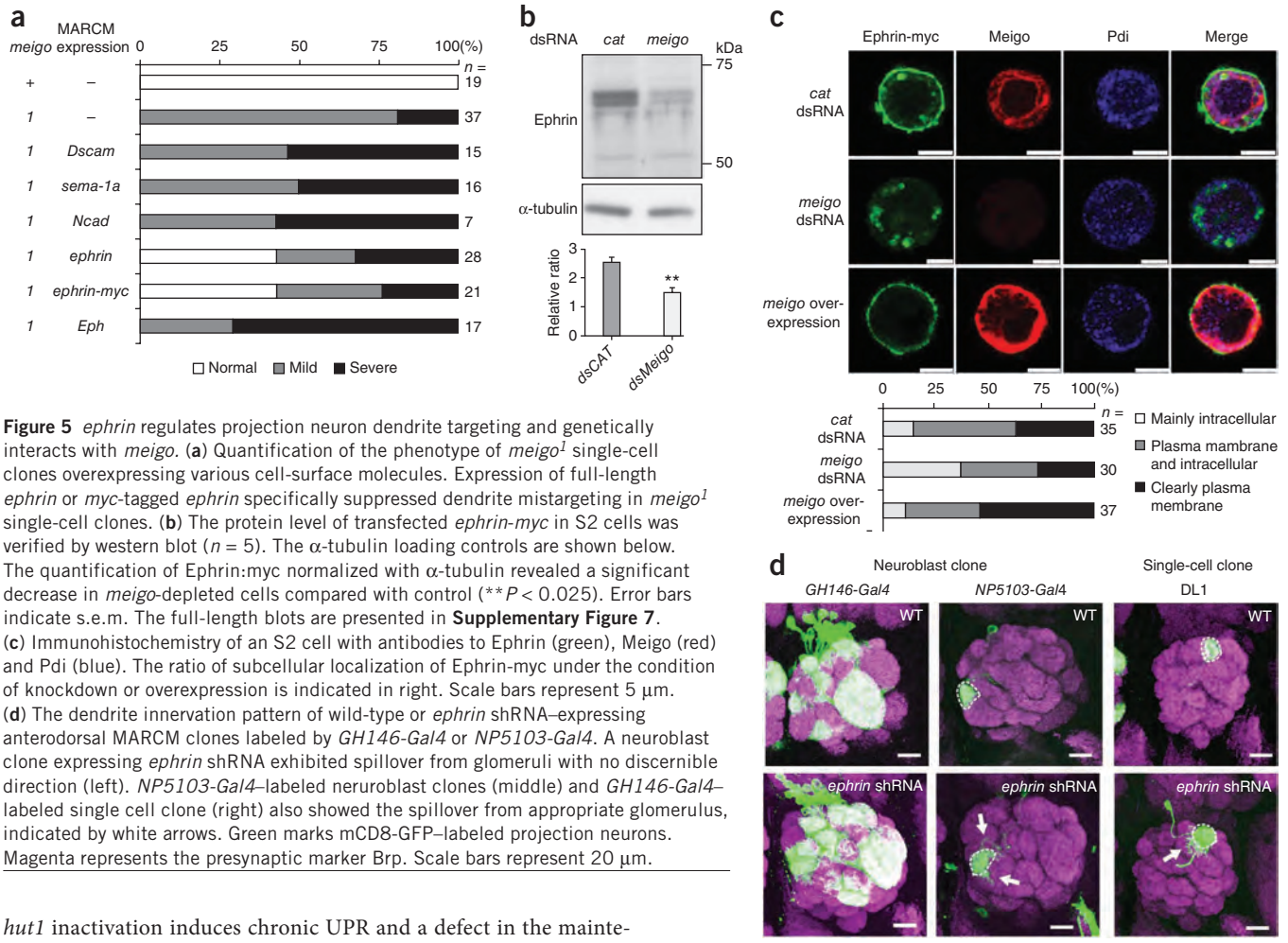

Figure 5 *ephrin* regulates projection neuron dendrite targeting and genetically interacts with *meigo*. (**a**) Quantification of the phenotype of *meigo*^{1} single-cell clones overexpressing various cell-surface molecules. Expression of full-length *ephrin* or *myc*-tagged *ephrin* specifically suppressed dendrite mistargeting in *meigo*^{1} single-cell clones. (**b**) The protein level of transfected *ephrin-myc* in S2 cells was verified by western blot ($n = 5$). The α-tubulin loading controls are shown below. The quantification of Ephrin:myc normalized with α-tubulin revealed a significant decrease in *meigo*-depleted cells compared with control (**$P < 0.025$). Error bars indicate s.e.m. The full-length blots are presented in **Supplementary Figure 7**. (**c**) Immunohistochemistry of an S2 cell with antibodies to Ephrin (green), Meigo (red) and Pdi (blue). The ratio of subcellular localization of Ephrin-myc under the condition of knockdown or overexpression is indicated in right. Scale bars represent 5 μm. (**d**) The dendrite innervation pattern of wild-type or *ephrin* shRNA–expressing anterodorsal MARCM clones labeled by *GH146-Gal4* or *NP5103-Gal4*. A neuroblast clone expressing *ephrin* shRNA exhibited spillover from glomeruli with no discernible direction (left). *NP5103-Gal4*–labeled neruroblast clones (middle) and *GH146-Gal4*–labeled single cell clone (right) also showed the spillover from appropriate glomerulus, indicated by white arrows. Green marks mCD8-GFP–labeled projection neurons. Magenta represents the presynaptic marker Brp. Scale bars represent 20 μm.

hut1 inactivation induces chronic UPR and a defect in the maintenance of ER structure, resulting in early developmental lethality[19]. On the contrary, in cultured cells, ER stress induced by dithiothreitol leads to upregulation of *meigo*[39] and the human homolog *UGTrel1* (ref. 40). Thus, Meigo could represent a conserved aspect of the UPR. To examine whether loss of Meigo causes a UPR in *Drosophila*, we generated double-stranded RNA against *meigo* (*meigo* dsRNA) to knockdown its endogenous expression in S2 cells. To detect UPR, we simultaneously expressed an *xbp1-EGFP* construct whose mRNA is unconventionally spliced following UPR, producing a fluorescent fusion protein[16,41]. Following application of *meigo* dsRNA (but not control dsRNA for *chloramphenicol acetyltransferase* (*cat*) of *E. coli.*), we detected the Xbp1-EGFP fusion protein, indicating the presence of a UPR (**Fig. 4a**). We also detected a significant increase in mRNA for *hsc3* (the *Drosophila* BiP) and *pdi* in S2 cells treated with *meigo* dsRNAs ($P < 0.05$; **Fig. 4b**). Furthermore, when *xbp1-egfp* was overexpressed in *meigo*^{1} projection neuron MARCM clones, the Xbp1-EGFP fusion protein was found in the nuclei (**Fig. 4c**), revealing a similarity between the *in vivo* and cell culture responses. The nuclear localization of Xbp1-EGFP reflects the fact that the Xbp1 protein is a transcription factor[16]. Notably, we also observed the upregulation of the ER chaperone Hsc3 in the dendrites of *meigo*^{1} projection neurons (**Fig. 4d**), suggesting that the UPR occurs not only in the cell body, but also in the dendrites locally.

Our finding that loss of Meigo induces a UPR suggests that the ER folding capacity is reduced in *meigo*^{1} projection neurons. To confirm this, we reduced ER folding capacity by expressing a dominant-negative form of *Hsc3* (*Hsc3*^{K97S}, *Hsc3*^{D231S})[42] or further induced ER stress by expressing *ninaE*^{G69D}, which encodes a mutant form of Rhodopsin-1 (Rh-1^{G69D})[16]. As above, MARCM expression of *Hsc3*^{K97S}, *Hsc3*^{D231S} or *ninaE*^{G69D} by *GH146-Gal4* had a mild effect on wild-type projection neuron dendrite targeting, but substantially enhanced dendrite mistargeting in *meigo*^{1} neurons (**Fig. 4e**; phenotype criteria in **Fig. 1e**). These findings suggest that wild-type projection neurons are capable of managing these artificial ER stress, whereas *meigo*^{1} projection neurons are vulnerable to ER stress, probably as a result of the reduced ER folding capacity.

ephrin genetically interacts with *meigo*

Why does the *meigo* abrogation associated with UPR cause such a specific targeting defect in projection neuron dendrites? We hypothesized that the functions of particular cell surface proteins governing projection neuron dendrite targeting are weakened in *meigo*^{1} projection neuron clones. To identify the hypothesized cell surface protein whose function is impaired in *meigo*^{1} projection neurons, we performed a genetic suppressor screen for projection neuron dendrite targeting and identified *ephrin* (**Supplementary Table 2**). Overexpression of *ephrin* specifically and substantially suppressed the dendrite refinement defect of *meigo*^{1} DL1 projection neuron single-cell clones (**Fig. 5a**). Notably, only the 'mild mistargeting class', the dendrite spillover from DL1 glomerulus, was suppressed, whereas the 'severe mistargeting class' (**Fig. 1e**) was mostly unchanged (**Fig. 5a**). In contrast, overexpression of other genes, including *sema-1a*, *DN-cadherin* and

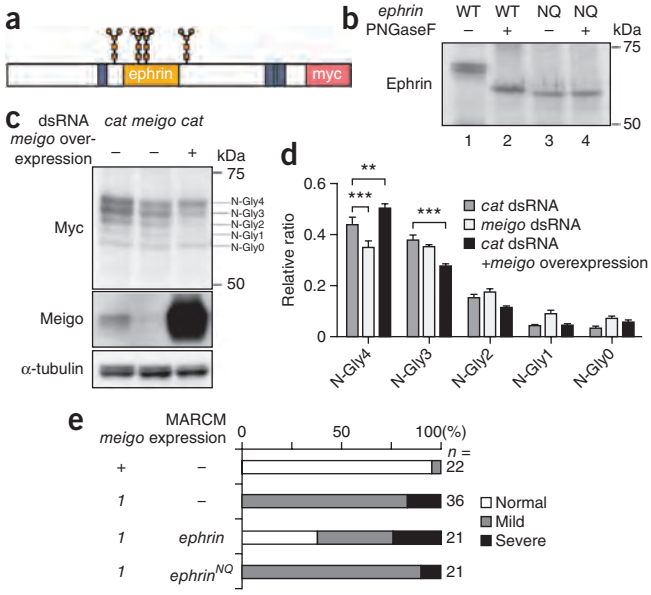

Figure 6 Meigo positively regulates the *N*-glycosylation of Ephrin that is important for its function *in vivo*. (**a**) Structure of the Ephrin-myc protein. The three transmembrane domains (gray boxes) and ephrin domain (orange box) are predicted. The four *N*-glycosylation sites are Asn222, Asn265, Asn274 and Asn365, which exist around the ephrin domain (orange branches). In Ephrin^{NQ}-myc, all of the *N*-glycosylation sites were mutated from Asn to Gln. The C terminus is fused with five copies of myc tags (pink bar). (**b**) *N*-glycosidase (PNGaseF) sensitivity of ephrin-myc or ephrin^{NQ}-myc expressed in S2 cells. The PNGaseF treatment to the ephrin-myc resulted in a band shift to the comparable molecular weight of ephrin^{NQ}-myc, indicating that ephrin-myc is *N*-glycosylated. (**c**) Immunoblot analysis showing the *N*-glycosylation state of ephrin-myc in either *meigo* knockdown or overexpression. The highest band (N-Gly4) represents all of the four predicted sites being *N*-glycosylated, the second highest band (N-Gly3) indicates that three sites are *N*-glycosylated, and so on. Middle, immunoblot with antibody to Meigo, which shows effective knockdown and overexpression of *meigo*. The α-tubulin loading controls are shown below. Full-length blots for the data shown in **b** and **c** are presented in **Supplementary Figure 7**. (**d**) Quantification of the relative ratio of N-Gly4, N-Gly3, N-Gly2, N-Gly1 and N-Gly0. Meigo positively regulated the ratio of N-Gly4 ($n = 5$ independent experiments, $^{**}P < 0.01$, $^{***}P < 0.001$). Error bars indicate s.e.m. (**e**) Quantification of the phenotype of *meigo*^{1} single-cell clones overexpressing *ephrin-myc* or *ephrin*^{NQ}*-myc*. The suppression efficiency was apparently weaker in *ephrin*^{NQ}*-myc* clones than in *ephrin-myc* clones.

Dscam, which are required for projection neuron dendrite targeting[7,9,11], did not suppress the dendrite refinement defect or targeting defect of *meigo*^{1} DL1 projection neurons (**Fig. 5a** and **Supplementary Table 2**). The overexpression of *Eph* in the *meigo*^{1} projection neuron enhanced the severity of the phenotype (**Fig. 5a**), suggesting that Eph-ephrin signaling contributes to the dendrite targeting and glomerular refinement of projection neuron.

Next, we tested whether Meigo can affect the amount of cell surface molecules that are expressed, including Ephrin. As we could not monitor endogenous Ephrin in projection neurons, owing to a lack of appropriate reagents, we quantified the expression of transfected Ephrin:myc, Sema-1a or DN-Cadherin[43] in control and *meigo* dsRNA–treated S2 cells. We detected, to different degrees, significant reductions in the expression of Ephrin-myc ($P < 0.025$), Sema-1a ($P < 0.05$) and DN-Cadherin ($P < 0.05$) proteins in *meigo* dsRNA–treated S2 cells compared with nontreated S2 cells (**Fig. 5b** and **Supplementary Fig. 3c**,**d**). Furthermore, the subcellular localization of Ephrin was also affected in *meigo* dsRNA–treated S2 cells (**Fig. 5c**). The ratio of cells with Ephrin-myc present at the plasma membrane was substantially decreased by knockdown of *meigo*, whereas the cell surface localization of Ephrin-myc was promoted in cells overexpressing *meigo* (**Fig. 5c**). These genetic and biochemical data suggest that dendrite targeting defect in *meigo*^{1} projection neurons seems to be, at least in part, a result of the reduction of Ephrin protein at the plasma membrane.

Ephrin is essential for glomerular refinement of dendrites

The *Drosophila ephrin* gene is located on the fourth chromosome, which prevented us from performing mutant MARCM analysis. To examine the requirement of *ephrin* in projection neuron dendrite targeting, we used MARCM to express short-hairpin RNA[44] for *ephrin* (*ephrin* shRNA; **Supplementary Fig. 4a–d**). The anterodorsal neuroblast projection neuron clones expressing *ephrin* shRNA (**Fig. 5d**) exhibited dendrite spillover, which was rescued by the expression of shRNA-resistant *ephrin* (*UAS-ephrin*^{resistant}; **Supplementary Fig. 4e**). We did not find preferential direction of the dendrite spillover, and the severity and penetrance of spillover seemed to be different between projection neuron classes (**Fig. 5d** and data not shown).

To analyze the dendrite defects in more detail, we analyzed single-cell clones of projection neurons innervating DL1 and neuroblast projection neuron clones innervating VM2. Notably, dendrites of DL1 or VM2 projection neurons expressing *ephrin* shRNA exhibited a spillover phenotype (**Fig. 5d**), which mimicked that of *meigo*^{1} projection neurons (*NP5103-Gal4*; **Fig. 1c**). Thus, Ephrin is indeed essential in projection neuron dendrites for their proper refinement into the glomerulus, which is a part of the phenotype of *meigo*^{1} projection neuron.

Meigo contributes to *N*-glycosylation of Ephrin

As Meigo is a putative NST that is required for the efficient production of cell surface molecules (**Fig. 5b** and **Supplementary Fig. 3c**,**d**), we expected that Meigo might regulate ER folding capacity through glycosylation machinery in the ER[45]. To examine this possibility, we analyzed the glycosylation of one of the target proteins, Ephrin. Ephrins are reported to have conserved *N*-glycosylation sites between family members and species, and the *N*-glycosylation of mouse Ephrin has been reported *in vivo*[46]. However, the role of *N*-glycosylation of the Ephrin protein has not yet been characterized. For the *Drosophila* Ephrin, the NetOGlyc 3.1 (http://www.cbs.dtu.dk/services/NetOGlyc/) and NetNGlyc 3.1 (http://www.cbs.dtu.dk/services/NetNGlyc/) servers predicted no site for *O*-glycosylation and four potential sites (Asn-222, Asn-265, Asn-274 and Asn-365) for *N*-glycosylation (**Fig. 6a**). We confirmed that these sites were indeed *N*-glycosylated. Western blotting analysis with cell lysate extracted from S2 cells expressing Ephrin-myc showed four bands around 60 to 70 kDa (**Fig. 6b**). Treatment of cell extracts with the *N*-glycosydase PNGaseF resulted in the band shift to the smallest molecular weight of about 60 kDa (**Fig. 6b**), and mutagenesis of each potential *N*-glycosylation site caused the absence of the highest molecular weight band (**Supplementary Fig. 5**). Mutation of all putative *N*-glycosylation sites (Ephrin^{NQ}) resulted in a single band that was approximately the same molecular weight as seen after PNGaseF treatment (**Fig. 6b**), suggesting that Ephrin is *N*-glycosylated and that the four bands of Ephrin-myc correspond to the *N*-glysosylation state of Ephrin-myc.

Next, we examined whether Meigo is required for *N*-glycosylation of Ephrin in S2 cells. We transiently expressed *ephrin-myc* in *meigo* dsRNA–treated S2 cells and analyzed the *N*-glycosylation state of Ephrin-myc. We reproducibly detected that the relative amount of the fully *N*-glycosylated form (N-Gly4) of Ephrin-myc (band at the

highest molecular weight) was significantly reduced in S2 cells treated with *meigo* dsRNA compared with those treated with control dsRNA ($P < 0.001$; **Fig. 6c**,**d**). In contrast, overexpression of *meigo* resulted in a significant increase in the amount of *N*-glycosylation of Ephrin-myc ($P < 0.01$; **Fig. 6c**,**d**). These results indicate that Meigo positively affects the *N*-glycosylation state of Ephrin.

Finally, to examine the effect of *N*-glycosylation on signaling ability, we used a transgene expressing a form of Ephrin in which all of the *N*-glycosylation sites were mutated, *UAS–ephrin^{NQ}-myc*. We found that Ephin^{NQ}-myc could not suppress the dendrite refinement defect of *meigo^{1}* projection neurons (**Fig. 6e**), suggesting that *N*-glycosylation of Ephrin is crucial for its effective function *in vivo*. Thus, Meigo-mediated *N*-glycosylation is required for the effective function of Ephrin *in vivo*.

DISCUSSION

Possible functions of Meigo in neuronal targeting

The loss-of-function *meigo* phenotype suggests that *meigo* has two functions in the projection neuron: dendrite targeting along the mediolateral axis of the antennal lobe and refinement of dendrites of individual projection neurons into single glomerulus. We propose that Meigo-mediated ER folding capacity is required for the spatio-temporal expression and function of various cell surface molecules (**Supplementary Fig. 6**). Among such molecules, however, only some may be susceptible to the reduction of ER folding capacity, accounting for the exquisitely specific phenotype of *meigo^{1}* projection neurons and ORNs. We identified Ephrin as one such receptor that regulates the glomerular refinement of projection neuron dendrites. In the dendrites of *meigo^{1}* projection neuron, Ephrin protein level was reduced, it was not localized to the cell surface efficiently and it was not fully *N*-glycosylated, all of which would cause the impairment of Ephrin function (**Supplementary Fig. 6**). The dendrite targeting defect along the mediolateral axis of *meigo^{1}* projection neurons is not a consequence of the refinement defect, as *ephrin* overexpression was able to suppress mild, but not severe, phenotypes, and projection neurons expressing *ephrin* shRNA exhibited only the refinement defect. The effector molecule(s) that regulate dendrite and axon targeting along the mediolateral axis require future investigation. In summary, our results provide an unexpected link between Meigo as a regulator of ER folding capacity, Ephrin function and neuronal targeting specificity.

Consistent with previous studies of *meigo* homologs, we found that *Drosophila* Meigo strongly contributed to the UPR in cultured cells and *in vivo*. In addition, we also found that the putative NST Meigo positively regulated the *N*-glycosylation state of Ephrin, one of the target molecules. Because *N*-glycan is important for protein folding and quality control, the impairment of *N*-glycan synthesis often causes a UPR[45]. Although we could not exclude the possibility that Meigo directly contributes to the protein folding process, the mutant MARCM clones for *ero1l,* which is important for disulfide bond formation[47], did not exhibit the same dendrite targeting defect as *meigo*. Thus, it is reasonable to speculate that Meigo is primarily required for an aspect of protein *N*-glycosylation, and Meigo knockdown results in less ER folding capacity, accompanied by a UPR.

How does Meigo contribute to protein *N*-glycosylation? One possible function is UDP-glucose transporter activity, as with the plant ortholog[48], which can be linked to the glucosylation of *N*-glycan. As glucose is thought to be supplied from glucose phosphate dolichol in the ER for the glucosylation of *N*-glycan, this possibility also affects the glycobiological field. The other possibilities are that Meigo may function in core *N*-glycan synthesis or in translocation to the nascent polypeptides. Given that the mutant MARCM projection neuron clone for *DSiaT* exhibited the dendrite spillover phenotype, the sialylation of *N*-glycan might be important for the glomerular refinement[33]. In each case, further biochemical studies are required to reveal the precise molecular function of Meigo.

Neural targeting requires proper ER folding capacity

Precise neural circuit assembly is achieved by the combinatorial and sequential use of cell surface receptors and ligands, which are largely synthesized and folded in the ER. Thus, a proper folding capacity of the ER is critical for neural circuit formation, but the *in vivo* regulation of such has not been investigated. Using genetic mosaic methods, we found that induction of ER stress solely in the wild-type projection neurons did not cause dendrite mistargeting. This suggests that ER folding capacity is large enough and/or the UPR works efficiently enough to overcome ER stress without disturbing the function of cell surface receptors and ligands. On the other hand, the specific targeting defect observed in *meigo^{1}* mosaic clones accompanied by a UPR was heightened by the further enhancement of ER stress. Thus, we present a broadly applicable hypothesis: Meigo-mediated ER folding capacity affects proteins involved in neural wiring. When *meigo* is absent, the ER folding capacity is reduced so that the translational attenuation through the UPR occurs severely. Meigo can provide unique inroads to investigate the unanticipated role of ER homeostasis in neural circuit formation.

Facilitation of Ephrin function by Meigo

Our genetic data suggest that, at least in projection neuron dendrites, Ephrin is involved in the refinement into the proper glomeruli. Ephrin has been implicated in axon target selection in mammalian olfactory system[49]. We found that Ephrin was also required for dendrite targeting. In addition, our results provide evidence that Meigo-mediated *N*-glycosylation of Ephrin is likely to be important for its function *in vivo*.

Although we cannot completely rule out the possibility that Meigo and Ephrin independently contribute to dendrite targeting specificity, several lines of evidence support the notion that Meigo promotes the Ephrin signal for dendrite refinement. First, *meigo* and *ephrin* exhibited strong genetic interactions in projection neuron dendrite targeting. Second, both *meigo^{1}* projection neurons and *ephrin* shRNA–expressing projection neurons exhibited a similar phenotype in respect to dendrite spillover. Third, as Ephrin is a transmembrane protein, it is presumed to pass through the ER, where Meigo functions. Indeed, *meigo* knockdown in S2 cells led to a substantial reduction in Ephrin protein level, impairment of cell surface transport and reduced *N*-glycosylation state, indicating that Meigo is required for the efficient function of Ephrin proteins.

Why was the dendrite refinement defect of *meigo^{1}* projection neuron specifically suppressed by *ephrin* overexpression? One possibility is that the Ephrin protein is highly sensitive to ER status. The UPR in *meigo^{1}* projection neurons is unlikely to be prohibitively severe because the axonal morphology and size of *meigo^{1}* neuroblast clones were largely normal (data not shown). Thus, such a mild ER stress may sufficiently affect the function of ER stress-sensitive proteins such as Ephrin, but not that of other transmembrane proteins. This is consistent with the fact that *meigo^{1}* projection neurons are apparently sensitized to ER stress caused by *ninaE^{G69D}* or dominant-negative *Hsc3* overexpression. The other possibility is that the *N*-glycosylation modulated by Meigo might be critical for Ephrin compared with the other cell surface molecules. To the best of our knowledge, our results provide the first evidence that *N*-glycosylation of Ephrin is important for its function *in vivo*.

Synaptic partners detect mediolateral axis independently

Coarse targeting of adult projection neuron dendrites along the dorsolateral to ventromedial axis of the antennal lobe is partially determined by the projection neuron receptor Sema-1a detecting Sema-2a/b[7,8]. No additional axis in the antennal lobe for constructing the local olfactory circuit has been identified. In this study, we found that dendrites of *meigo*^{1} projection neurons and axons of *meigo*^{1} ORNs exhibited medial mistargeting in the antennal lobe. Furthermore, Meigo, an ER protein, modulated targeting along the mediolateral axis. Thus, our findings confirm and strengthen the concept that the wiring of local neural circuits is based on the positional information conveyed along several body axes. Moreover, these results provide substantial advances toward understanding the mechanisms of neural circuit formation in a three-dimensional brain structure. Note that the dendrite refinement defect observed in *ephrin* shRNA–expressing projection neurons is similar to a part of the phenotype of *meigo*^{1} projection neuron. This suggests that the regulation of Ephrin signal is only a part of Meigo's role in the dendrite morphogenesis; additional cell-surface molecules may account for Meigo-mediated mediolateral targeting of projection neuron dendrites and ORN axons.

To find their proper target, dendrites utilize receptors to recognize the cellular environments. Thus, it is reasonable that partners of presynaptic axons and postsynaptic dendrites share common molecules for targeting a shared destination. However, there has been no evidence that a common molecular mechanism is used independently by synaptic partners. Our data indicate that synaptic partners independently require the same molecule, Meigo, for their precise targeting. This is distinct from the Teneurins, which serve as synaptic partners, matching molecules by promoting projection neuron–ORN recognition[12,50]. Instead, Meigo likely mediates a coarse targeting process to bring partner projection neurons and ORNs to the same vicinity independently. This is then followed by a synaptic matching process mediated by molecules such as the Teneurins.

In summary, we found that neurite targeting to precise target regions is achieved by an analogous mechanism in both pre- and postsynaptic partners through recognition of mediolateral axial information and refinement into each glomerulus. Meigo seems to be required for enhancing the ER folding capacity, possibly through the *N*-glycosylation machinery. The efficient expression, cell surface transport and *N*-glycosylation of Ephrin were promoted by Meigo. Further investigation of the physiological function of Meigo and its contribution to the Ephrin signal will shed light on the regulatory mechanism for Ephrin function in the ER during neural circuit formation.

METHODS

Methods and any associated references are available in the online version of the paper.

Note: Supplementary information is available in the online version of the paper.

ACKNOWLEDGMENTS

We thank J.B. Thomas, Bloomington and the Kyoto *Drosophila* Stock Center for fly stocks, A.H. Brand (University of Cambridge) for the Ephrin antibody and fly stocks, S. Goto (Rikkyo University) for the dGLG1 (120 kDa) antibody, C. Field (Harvard University) for the Lava Lamp antibody, T. Uemura (Kyoto University) for the *UAS-DNcadherin* plasmid, H.D. Ryoo (New York University) and P.M. Domingos (Instituto de Tecnologia Química e Biológica) for xbp1:EGFP-related reagents and the Hsc3 antibody, C.-H. Chen for advice on constructing shRNAs, G. Thomas and M. Khanna for advice on performing OptiPrep density gradient centrifugation, and all of the members of the Miura and Luo laboratories for comments on this study. We especially thank T. Mosca for improving the manuscript and M. Okumura and T.C. for the blind test. L.L. is funded by the Howard Hughes Medical Institute. This work was supported by grants from the Ministry of Education, Culture, Sports, Science and Technology in Japan to M.M. and T.C., the Japan Society for the Promotion of Science to S.U.S., M.M. and T.C., the Japan Science and Technology Agency to M.M. and T.C., and the US National Institutes of Health (R01 DC005982) to L.L.

AUTHOR CONTRIBUTIONS

S.U.S. performed most of the experiments and analyzed the data. S.H., K.C. and T.K. assisted in some experiments. T.C. supervised the project. S.U.S. and T.C. wrote the paper with feedback from L.L. and M.M.

COMPETING FINANCIAL INTERESTS

The authors declare no competing financial interests.

1. Mumm, J.S. *et al. In vivo* imaging reveals dendritic targeting of laminated afferents by zebrafish retinal ganglion cells. *Neuron* **52**, 609–621 (2006).
2. Vrieseling, E. & Arber, S. Target-induced transcriptional control of dendritic patterning and connectivity in motor neurons by the ETS gene *Pea3*. *Cell* **127**, 1439–1452 (2006).
3. Jefferis, G.S. & Hummel, T. Wiring specificity in the olfactory system. *Semin. Cell Dev. Biol.* **17**, 50–65 (2006).
4. Spletter, M.L. *et al.* Lola regulates *Drosophila* olfactory projection neuron identity and targeting specificity. *Neural Dev.* **2**, 14 (2007).
5. Komiyama, T., Johnson, W., Luo, L. & Jefferis, G. From lineage to wiring specificity. POU domain transcription factors control precise connections of *Drosophila* olfactory projection neurons. *Cell* **112**, 157–167 (2003).
6. Jefferis, G.S. *et al.* Developmental origin of wiring specificity in the olfactory system of *Drosophila*. *Development* **131**, 117–130 (2004).
7. Komiyama, T., Sweeney, L., Schuldiner, O., Garcia, K. & Luo, L. Graded expression of semaphorin-1a cell-autonomously directs dendritic targeting of olfactory projection neurons. *Cell* **128**, 399–410 (2007).
8. Sweeney, L.B. *et al.* Secreted semaphorins from degenerating larval ORN axons direct adult projection neuron dendrite targeting. *Neuron* **72**, 734–747 (2011).
9. Zhu, H. & Luo, L. Diverse functions of N-cadherin in dendritic and axonal terminal arborization of olfactory projection neurons. *Neuron* **42**, 63–75 (2004).
10. Hong, W. *et al.* Leucine-rich repeat transmembrane proteins instruct discrete dendrite targeting in an olfactory map. *Nat. Neurosci.* **12**, 1542–1550 (2009).
11. Zhu, H. *et al.* Dendritic patterning by Dscam and synaptic partner matching in the *Drosophila* antennal lobe. *Nat. Neurosci.* **9**, 349–355 (2006).
12. Hong, W., Mosca, T. & Luo, L. Teneurins instruct synaptic partner matching in an olfactory map. *Nature* **484**, 201–207 (2012).
13. Ron, D. & Walter, P. Signal integration in the endoplasmic reticulum unfolded protein response. *Nat. Rev. Mol. Cell Biol.* **8**, 519–529 (2007).
14. Cudna, R.E. & Dickson, A.J. Endoplasmic reticulum signaling as a determinant of recombinant protein expression. *Biotechnol. Bioeng.* **81**, 56–65 (2003).
15. Schröder, M. & Kaufman, R.J. ER stress and the unfolded protein response. *Mutat. Res.* **569**, 29–63 (2005).
16. Ryoo, H.D., Domingos, P., Kang, M. & Steller, H. Unfolded protein response in a *Drosophila* model for retinal degeneration. *EMBO J.* **26**, 242–252 (2007).
17. Souid, S., Lepesant, J. & Yanicostas, C. The *xbp-1* gene is essential for development in *Drosophila*. *Dev. Genes Evol.* **217**, 159–167 (2007).
18. Haecker, A. *et al.* Wollknauel is required for embryo patterning and encodes the *Drosophila* ALG5 UDP-glucose:dolichyl-phosphate glucosyltransferase. *Development* **135**, 1745–1749 (2008).
19. Dejima, K. *et al.* The ortholog of human solute carrier family 35 member B1 (UDP-galactose transporter-related protein 1) is involved in maintenance of ER homeostasis and essential for larval development in *Caenorhabditis elegans*. *FASEB J.* **23**, 2215–2225 (2009).
20. Chihara, T., Luginbuhl, D. & Luo, L. Cytoplasmic and mitochondrial protein translation in axonal and dendritic terminal arborization. *Nat. Neurosci.* **10**, 828–837 (2007).
21. Tanaka, N.K., Awasaki, T., Shimada, T. & Ito, K. Integration of chemosensory pathways in the *Drosophila* second-order olfactory centers. *Curr. Biol.* **14**, 449–457 (2004).
22. Newsome, T.P., Asling, B. & Dickson, B. Analysis of *Drosophila* photoreceptor axon guidance in eye-specific mosaics. *Development* **127**, 851–860 (2000).
23. Kobayashi, T., Sleeman, J., Coughtrie, M. & Burchell, B. Molecular and functional characterization of microsomal UDP-glucuronic acid uptake by members of the nucleotide sugar transporter (NST) family. *Biochem. J.* **400**, 281–289 (2006).
24. Komiyama, T., Carlson, J. & Luo, L. Olfactory receptor neuron axon targeting: intrinsic transcriptional control and hierarchical interactions. *Nat. Neurosci.* **7**, 819–825 (2004).
25. Khanna, M.R., Stanley, B. & Thomas, G. Towards a membrane proteome in *Drosophila*: a method for the isolation of plasma membrane. *BMC Genomics* **11**, 302 (2010).
26. Papoulas, O., Hays, T. & Sisson, J. The golgin Lava lamp mediates dynein-based Golgi movements during *Drosophila* cellularization. *Nat. Cell Biol.* **7**, 612–618 (2005).

27. Ishida, N. & Kawakita, M. Molecular physiology and pathology of the nucleotide sugar transporter family (SLC35). *Pflugers Arch.* **447**, 768–775 (2004).
28. Goto, S. *et al.* UDP-sugar transporter implicated in glycosylation and processing of Notch. *Nat. Cell Biol.* **3**, 816–822 (2001).
29. Lüders, F. *et al.* Slalom encodes an adenosine 3′-phosphate 5′-phosphosulfate transporter essential for development in *Drosophila*. *EMBO J.* **22**, 3635–3644 (2003).
30. Selva, E.M. *et al.* Dual role of the fringe connection gene in both heparan sulphate and fringe-dependent signaling events. *Nat. Cell Biol.* **3**, 809–815 (2001).
31. Ishikawa, H.O. *et al.* Two pathways for importing GDP-fucose into the endoplasmic reticulum lumen function redundantly in the *O*-fucosylation of Notch in *Drosophila*. *J. Biol. Chem.* **285**, 4122–4129 (2010).
32. Lin, Y.R., Reddy, B. & Irvine, K. Requirement for a core 1 galactosyltransferase in the *Drosophila* nervous system. *Dev. Dyn.* **237**, 3703–3714 (2008).
33. Repnikova, E. *et al.* Sialyltransferase regulates nervous system function in *Drosophila*. *J. Neurosci.* **30**, 6466–6476 (2010).
34. Lin, X. & Perrimon, N. Dally cooperates with *Drosophila* Frizzled 2 to transduce Wingless signaling. *Nature* **400**, 281–284 (1999).
35. Takei, Y., Ozawa, Y., Sato, M., Watanabe, A. & Tabata, T. Three *Drosophila* EXT genes shape morphogen gradients through synthesis of heparan sulfate proteoglycans. *Development* **131**, 73–82 (2004).
36. Kamimura, K. *et al.* Specific and flexible roles of heparan sulfate modifications in *Drosophila* FGF signaling. *J. Cell Biol.* **174**, 773–778 (2006).
37. Léonard, R. *et al.* The *Drosophila* fused lobes gene encodes an *N*-acetylglucosaminidase involved in *N*-glycan processing. *J. Biol. Chem.* **281**, 4867–4875 (2006).
38. Nakanishi, H. *et al.* Hut1 proteins identified in *Saccharomyces cerevisiae* and *Schizosaccharomyces pombe* are functional homologues involved in the protein-folding process at the endoplasmic reticulum. *Yeast* **18**, 543–554 (2001).
39. Hollien, J. & Weissman, J.S. Decay of endoplasmic reticulum-localized mRNAs during the unfolded protein response. *Science* **313**, 104–107 (2006).
40. Murray, J.I. *et al.* Diverse and specific gene expression responses to stresses in cultured human cells. *Mol. Biol. Cell* **15**, 2361–2374 (2004).
41. Iwawaki, T., Akai, R., Kohno, K. & Miura, M. A transgenic mouse model for monitoring endoplasmic reticulum stress. *Nat. Med.* **10**, 98–102 (2004).
42. Elefant, F. & Palter, K. Tissue-specific expression of dominant negative mutant *Drosophila* HSC70 causes developmental defects and lethality. *Mol. Biol. Cell* **10**, 2101–2117 (1999).
43. Iwai, Y. *et al.* Axon patterning requires DN-cadherin, a novel neuronal adhesion receptor, in the *Drosophila* embryonic CNS. *Neuron* **19**, 77–89 (1997).
44. Chen, C.H. *et al.* A synthetic maternal-effect selfish genetic element drives population replacement in *Drosophila*. *Science* **316**, 597–600 (2007).
45. Lehrman, M.A. Stimulation of *N*-linked glycosylation and lipid-linked oligosaccharide synthesis by stress responses in metazoan cells. *Crit. Rev. Biochem. Mol. Biol.* **41**, 51–75 (2006).
46. Toth, J. *et al.* Crystal structure of an ephrin ectodomain. *Dev. Cell* **1**, 83–92 (2001).
47. Tien, A.C. *et al.* Ero1L, a thiol oxidase, is required for Notch signaling through cysteine bridge formation of the Lin12-Notch repeats in *Drosophila melanogaster*. *J. Cell Biol.* **182**, 1113–1125 (2008).
48. Reyes, F. *et al.* The nucleotide sugar transporters AtUTr1 and AtUTr3 are required for the incorporation of UDP-glucose into the endoplasmic reticulum, are essential for pollen development and are needed for embryo sac progress in *Arabidopsis thaliana*. *Plant J.* **61**, 423–435 (2010).
49. Cutforth, T. *et al.* Axonal ephrin-As and odorant receptors: coordinate determination of the olfactory sensory map. *Cell* **114**, 311–322 (2003).
50. Mosca, T.J., Hong, W., Dani, V., Favaloro, V. & Luo, L. Trans-synaptic Teneurin signaling in neuromuscular synapse organization and target choice. *Nature* **484**, 237–241 (2012).

ONLINE METHODS

Fly strains. The genotypes of *Drosophila melanogaster* used in each experiment are shown in **Supplementary Table 3**. Flies were maintained under standard laboratory condition (25 °C). The light-dark cycle was not controlled or monitored. The following mutants and transgenic lines were used: *y w; FRT^{2A}FRT^{82B}meigo^{1} y(+)/ TM6B Tb, y w; UAS-meigo^{WT}, CG5802^{KG01634}* (Bloomington stock center), *y w; FRT^{2A}fringe connection (frc)^{RY34}, UAS-frc, y w; FRT^{2A}slalom^{24533}, UAS-slalom, Efr^{3}, UAS-Efr-N-HA, UAS-Gfr-HA, C1GalTA$^{2.1}$, UAS-C1GalTA, fdl^{P}* (Bloomington stock center), *sfl$^{l(3)03844}$, y w; DSiaT^{S23}, FRT^{42D}ttv^{524}botv^{510}, FRT^{42D}sotv$^{32.6}$, Hs6st^{d770}, FRT^{82B}dar3(sar1)$^{11\text{-}3\text{-}6}$, rab1^{e0128}, sar1^{P1}, γCOP^{Δ1142}, xbp1^{k13803}, UAS-xbp1-egfp, UAS-ninaE^{G69D}, Ero1-like^{23T}FRT^{2A}, wol^{1}, wol^{2}, UAS-wol, UAS-Hsc3^{K97S}, UAS-Hsc3^{D231S}, dally^{80}, dally-like protein^{A187}, syndecan^{Df48}, ubi-Sara, trol^{null}, UAS-DNcadherin, UAS-Dscam-GFP, UAS-semaphorin-1a FRT^{40A}, UAS-plexinA-HA, robo^{GA285}, robo^{Z3127}, robo2^{1}, robo3^{1}, UAS-robo2, UAS-robo3, derailed^{R343}, derailed-2^{E124}, dystroglycan$^{Df(3R)618}$, UAS-eph*-myc, *DVAP-33A^{Δ448}FRT^{19A}, UAS-flag-dVAP-HA, exn^{EYΔ23}, dock^{P1}, FRT^{82B}pak^{16}, UAS-ephrin, UAS-ephrin-myc, UAS-ephrin^{Resistant}-myc, UAS-CG14511-shRNA, UAS-Csat-shRNA, UAS-CG14040-shRNA, UAS-ephrin-shRNA, UAS-eph-shRNA*. The original papers of mutants and transgenic flies are listed in **Supplementary Tables 1** and **2**.

Immunostaining. MARCM and brain immunostaining of both genders were performed as described[51,52]. Both genders of adult flies younger than 7 d were used. S2 cells (1×10^5) were grown for 2 h at 26 °C on coverslips, and were fixed for 20 min in 4% paraformaldehyde (wt/vol) with 0.3% Triton X-100 (vol/vol) in phosphate-buffered saline (PBST), and rinsed in PBST. Cells were subsequently blocked in PBST with 5% normal goat serum (vol/vol) for 30 min. Primary and secondary antibody incubation were carried out in blocking solution for 1 h at 20–25 °C, with three 10-min washes in PBST after each incubation. For antibodies, we used rat antibody to Meigo (1:250), rat antibody to mCD8 (1:100, Invitrogen, MCD0800), mouse antibody to Bruchpilot (1:100, Developmental Studies Hybridoma Bank (DSHB), nc82), rat antibody to DN-cadherin (1:40, DSHB, DNEX-8), rat antibody to dGLG1 (120 kDa)[53] (1:20, a gift from S. Goto, Rikkyo University), mouse antibody to KDEL (1:100, Stressgen, SPA-827), mouse antibody to Pdi (1:1,000, StressGen, SA-891), mouse antibody to GFP (1:1,000, Clontech, 632381), rabbit antibody to Hsc3 (1:200, a gift from H.D. Ryoo, New York University)[16], and rabbit antibody to Dephrin (1:1,000, a gift from A.H. Brand, University of Cambridge)[54]. For detecting endogenous Hsc3 in the brain, or endogenous Meigo and overexpressed Ephrin in S2 cells, Can Get Signal solution A (TOYOBO) was used according to the manufacturer's instructions. Triple-labeling experiments with antibodies to mCD8 (rat), GFP (mouse) and Brp (mouse) (described above) were carried out with the Zenon Alexa Fluor 647 mouse IgG1 labeling kit (Molecular Probes), diluted in PBST.

Statistical analysis. Statistical tests were performed using Prism 5 (GraphPad Software). For the quantification of projection neuron dendrites and ORN axons, quantification of mRNA level of UPR target genes, and quantification of protein level of Ephrin-myc, Sema-1a and DN-cadherin, we used the Mann Whitney test. For quantification of the relative ratio of five bands in **Figure 6d**, we used two-way repeated-measures ANOVA and Bonferroni post-tests. The number of biologically independent experiments and *P* values are indicated in the figure legends. The sample sizes were chosen according to standard practice in the field.

Projection neuron phenotype quantification. For the quantification of projection neuron dendrites, we imaged the MARCM anterodorsal neuroblast clones labeled by *GH146-Gal4* using an LSM5 PASCAL confocal microscope (Carl Zeiss) with an EC Plan-NEOFLUAR 40×/1,3 oil differential interference contrast lens (Carl Zeiss) and Immersol 518F (Carl Zeiss) immersion oil. The two-dimensional projection was derived from a confocal stack and dendrite termini were manually selected. The picture was rotated along the axis in question and a scale from 0 to 1 was overlaid, whereby the most medial or ventral corresponded to 0 and the most lateral or dorsal corresponded to 1 so as to maximally cover the antennal lobe. The relative amount of fluorescence along this scale was calculated. The mean positions of dendrite distribution were plotted as a graph and the average of the mean positions for each genetic manipulation was calculated. For the ORN axon quantification, the MARCM clones labeled by *pebbled-Gal4* were imaged and calculated as above. Image processing was done using ImageJ (US National Institutes of Health). For DL1 projection neuron classification, the genotypes of the stacked images of the DL1 projection neurons were blinded to avoid experiment bias. The investigator who conducted the blind tests shown in **Figures 1e**, **4e** and **5a** and the investigator who conducted the blind test shown in **Figure 6e** were totally independent from the investigator who performed the experiments.

Identification of the *meigo* mutation. The MARCM-based mosaic screen and single-nucleotide polymorphism mapping methods leading to the identification of *meigo^{1}* were analogous to those previously described[20]. Detailed mapping procedure is available on request.

Bioinformatics. For homology searches, we used InParanoid: Eukaryotic Ortholog Groups (http://inparanoid.sbc.su.se/cgi-bin/index.cgi). Identity and similarity were calculated by GENETYX-MAX. The Meigo structure was analyzed using the SOSUI server (http://bp.nuap.nagoya-u.ac.jp/sosui/). The proteins predicted to have NST activity were searched in Flybase (http://flybase.org/), and ClustalW (http://clustalw.ddbj.nig.ac.jp/top-j.html) was used to generate a phylogenetic tree of the putative *Drosophila* NSTs (**Fig. 3**).

Generation of Meigo antibody. Monoclonal rat antibody to Meigo was generated by immunization with a synthetic KLH conjugated peptide (CVFAALFVDML YGKKAPLATAKKPPVEGKLSEEKKLNS) corresponding to the C terminus of Meigo (Hokudo). The antibodies were purified by affinity to the antigen peptides and used for immunostaining and western blot.

DNA construction. To generate *UAS-meigo*, we obtained *meigo* cDNA from a cDNA library extracted from S2 cells. The *meigo* fragment was amplified using the following primers: 5′-CTTTAAAAACCGTCATCTGCCCG CC-3′ and 5′-GAAAATAAGTTGCCTTTGTTAGGC-3′. The PCR product was then subcloned into the *pT7Blue* vector by TA cloning. The fragment containing the entire cDNA was then cut from the vector using XbaI and KpnI and subcloned into the *pUAST* vector. To generate *UAS* shRNA for each gene, we followed a protocol[44] kindly provided by C.H. Chen (National Health Research Institute). The target sequences of the shRNAs are as follows: *CG14511* shRNA (5′-GCCAGGGAAGCGTTGTATTACA-3′ and 5′-GTGCCCCTAATCCTGCTATACT-3′), *Csat* shRNA (5′-TTACTCG CACAGTGTTTTAAGA-3′ and 5′-AACGCCAATACGCTGAAGTACA-3′), *CG14040* shRNA (5′-CAGCTGCAATCACATAATAAAA-3′ and 5′-GGGCA TACTATTCCAAATTATC-3′), *ephrin* shRNA (5′-AAGCAAGTTTCAA GGTTTTAAC-3′), *eph* shRNA (5′-GAACTCCGATGTAGATATTAAC-3′ and 5′-TAATGGATTTGGCTCTTATAGT-3′ and 5′-GGACCCACAAA CACAAATAATG-3′). Multiple sequences for a single gene means that multiple shRNAs are connected and subcloned into *pUAST* or *pUAST-attB* vectors. The mutant forms of *UAS–ephrin-myc* were generated using the QuickChange procedure (Stratagene). Primer sequences used for mutagenesis are available on request.

Cell culture and transfection. S2 cells were grown at 26 °C in Schneider's medium supplemented with 10% heat-inactivated fetal bovine serum (vol/vol), 100 U ml^{-1} penicillin and 100 μg ml^{-1} streptomycin. Cells in six-well plates (1×10^6 cells per well) were transfected using the Effectene Transfection Reagent (Qiagen #301425) according to the manufacturer's instructions. We used 400 ng per well of *Actin-Gal4* (pAcPa-Actin5c-GAL4) as a driver for each *UAS* transgene (400 ng per well for *UAS-meigo*, 200 ng per well for *UAS-Sema1a* or *UAS-DNcadherin* (gift from T. Uemura, Kyoto University) and 100 ng per well for *UAS–ephrin-myc*).

dsRNA treatment. Templates were generated by PCR amplification of the full-length *meigo* and *chloramphenicol acetyltransferase* (*cat*) genes using 5′ and 3′ primers that contained T7 and T3 consensus site and gene sequences. dsRNA for bacterial *cat* was used as a negative control because it is not expressed in *Drosophila* S2 cells. The PCR fragments were then used as templates for *in vitro* transcription by T7 RNA polymerase or T3 RNA polymerase (Promega) for 2 h at 37 °C. The synthesized single-stranded RNA was then hybridized with single-stranded RNA of a complementary sequence to obtain the double-stranded RNA. For dsRNA treatment of S2 cells, the cells were plated in six-well plates (cell density, 10^6 cells per well). 30 mg of dsRNA were transfected using the Effectene Transfection Reagent (Qiagen #301425) for effective internalization of dsRNA,

doi:10.1038/nn.3389

and cells were allowed to grow at 26 °C for 4 d. Cells were collected and used for the western blots in **Figure 4a** and the quantitative RT-PCR in **Figure 4b**. For the other western blots, the dsRNA-treated S2 cells were further transfected with dsRNA, *Actin-Gal4* and *UAS* transgenes (*UAS–xbp1-EGFP*, *UAS–ephrin-myc*, *UAS-meigo*, *UAS–sema-1a* or *UAS–DN-cadherin*). The cells were lysed with SDS sample buffer (2% SDS (wt/vol), 80 mM Tris-HCl (pH 6.8), 15% glycerol (vol/vol), 0.0025% Brilliant blue FCF (wt/vol), 2% 2-mercaptoethanol (vol/vol)) for the western blot (see below).

Western blot analysis. We subjected 5–10 μg of S2 cell lysates to SDS-PAGE analysis (10.5% for BiP, Lava Lamp, Sema-1a, DN-cadherin and Ephrin-myc detection by antibody to Myc; for others, 12.5%) and immunoblotting. Treatment with PNGase F (New England Biolabs) was performed according to the manufacture's instruction. Rat monoclonal antibody to Meigo (1:250), mouse monoclonal antibody to GFP (Clontech, 632381, 1:1,000), mouse monoclonal antibody to α-tubulin (Sigma, T6199, 1:5,000), rat monoclonal antibody to BiP (1:20,000, Babraham Institute, BT-GB-143P), rabbit polyclonal antibody to Lava Lamp[26] (1:3,000; a gift from C. Field, Harvard University), mouse antibody to Myc (1:2,000, Invitrogen, 46-0603), rabbit monoclonal antibody to Sema-1a and rat monoclonal antibody to DN-cadherin (1:200, DSHB, DNEX-8) were used as primary antibodies, whereas horseradish peroxidase–conjugated antibody to rabbit (1:1,000, Cell Signaling, #7074S), antibody to mouse (1:2,000, Promega, W402B) and antibody to rat (1:500, Jackson ImmunoResearch, 912-036-153) were used as secondary antibodies. ECL-plus Western Blotting Detection Reagents (Amersham) were used for detection. For quantification of bands, the average of three equally applied lanes was counted for $n = 1$, and independent experiments were performed more than three times. The intensities of bands were quantified using ImageJ and basically normalized with the intensity of α-tubulin. For the quantification of relative ratio of each band (N-Gly 4, 3, 2, 1 and 0) shown in **Figure 6d**, the intensities of each band were normalized by the total intensity of the five bands.

Quantitative RT-PCR analysis. dsRNA-treated S2 cell lysates were collected and the total RNA was extracted using TRIzol (Ambion). cDNA synthesis was performed using the PrimeScript RT Reagent Kit with gDNA Eraser (TaKaRa) according to the manufacturer's protocol. Expression of UPR target genes was analyzed by performing PCR using the original cDNA, SYBR Premix Ex TaqII (Tli RNaseH Plus) (TaKaRa) and the following primers: *hsc3* (5′-CGAGGAGAAGAAGGAAAAGGA-3′ and 5′-CGTCCGTTCTTGTACACACC-3′), *pdi* (5′-TTCGTGCTGGTCGAGTTCTA-3′ and 5′-CTTCTCGGCCAGTTGCTG-3′), *herp* (5′-ATCTCTTATCTATCCTGGCAAACC-3′ and 5′-TCATCTAATAGCTTGCCCGAGT-3′), *edem1* (5′-TGACCATGCCCATAATTGAA-3′ and 5′-TTGTTTCGGGGTTTTTGCT-3′), *edem2* (5′-GGGAATGCCACGTTTAGC-3′ and 5′-TTTTCAGGAAAAAGCCTATTTGA-3′). Light cycler 480 (Roche) was used for quantitative PCR.

Density gradient centrifugation. Density gradient centrifugation was carried out essentially as described[25,26]. 1.5–3.0 g of embryos (w^{1118}, 6–18 h old) were dechorionated in 50% bleach, thoroughly rinsed and carefully homogenized in ten volumes of homogenization buffer I (HB-I, 0.22 M sucrose, 0.12 M mannitol, 1 mM EDTA and 10 mM tricine, pH 7.2) containing 1× protease inhibitor cocktail (Complete, Roche) by 15 strokes of Pestle A in a Kontes homogenizer on ice. The initial homogenate was centrifuged at 3,000*g* for 10 min at 4 °C to pellet nuclei, 10,000*g* for 30 min at 4 °C to pellet mitochondria and at 100,000*g* for 1 h to obtain a microsome pellet. The microsome pellet was resuspended and mixed with OptiPrep (Accurate Chemical and Scientific) such that a 20–30% gradient was created with a total protein content of 12–15 mg per gradient. Centrifugation was at 70,000*g* for 12 h. We collected 0.25-ml fractions from the top of the tube for further analysis.

Quantification of subcellular localization in S2 cells. The S2 cells transiently transfected with *Actin-Gal4* and *UAS-ephrin-myc* with or without *UAS-meigo*, in addition to the dsRNA treatment, were stained and imaged using TCS-SP5 confocal microscope (Leica) with a PL APO CS 40×/ 0.85 CORR HCX oil lens (Leica) and GaAsP Hybrid Detection System (Leica). Fields of view were randomly selected and all of the cells expressing ephrin-myc within the field of view were imaged. For each experiment, more than ten cells were imaged and each biologically independent experiment was repeated three times. Prior to classification, the experimental conditions and Meigo staining of the images were blinded to avoid experimental bias. The investigator who conducted the blind test was totally independent from the investigator who performed experiments.

51. Lee, T. & Luo, L. Mosaic analysis with a repressible cell marker for studies of gene function in neuronal morphogenesis. *Neuron* **22**, 451–461 (1999).
52. Wu, J.S. & Luo, L. A protocol for mosaic analysis with a repressible cell marker (MARCM) in *Drosophila*. *Nat. Protoc.* **1**, 2583–2589 (2006).
53. Yamamoto-Hino, M. *et al.* Cisterna-specific localization of glycosylation-related proteins to the Golgi apparatus. *Cell Struct. Funct.* **37**, 55–63 (2012).
54. Bossing, T. & Brand, A. Dephrin, a transmembrane ephrin with a unique structure, prevents interneuronal axons from exiting the *Drosophila* embryonic CNS. *Development* **129**, 4205–4218 (2002).

Meigo governs dendrite targeting specificity by modulating Ephrin level and *N*-glycosylation

Sayaka U. Sekine, Shuka Haraguchi, Kinhong Chao, Tomoko Kato, Liqun Luo, Masayuki Miura, and Takahiro Chihara

Supplementary information

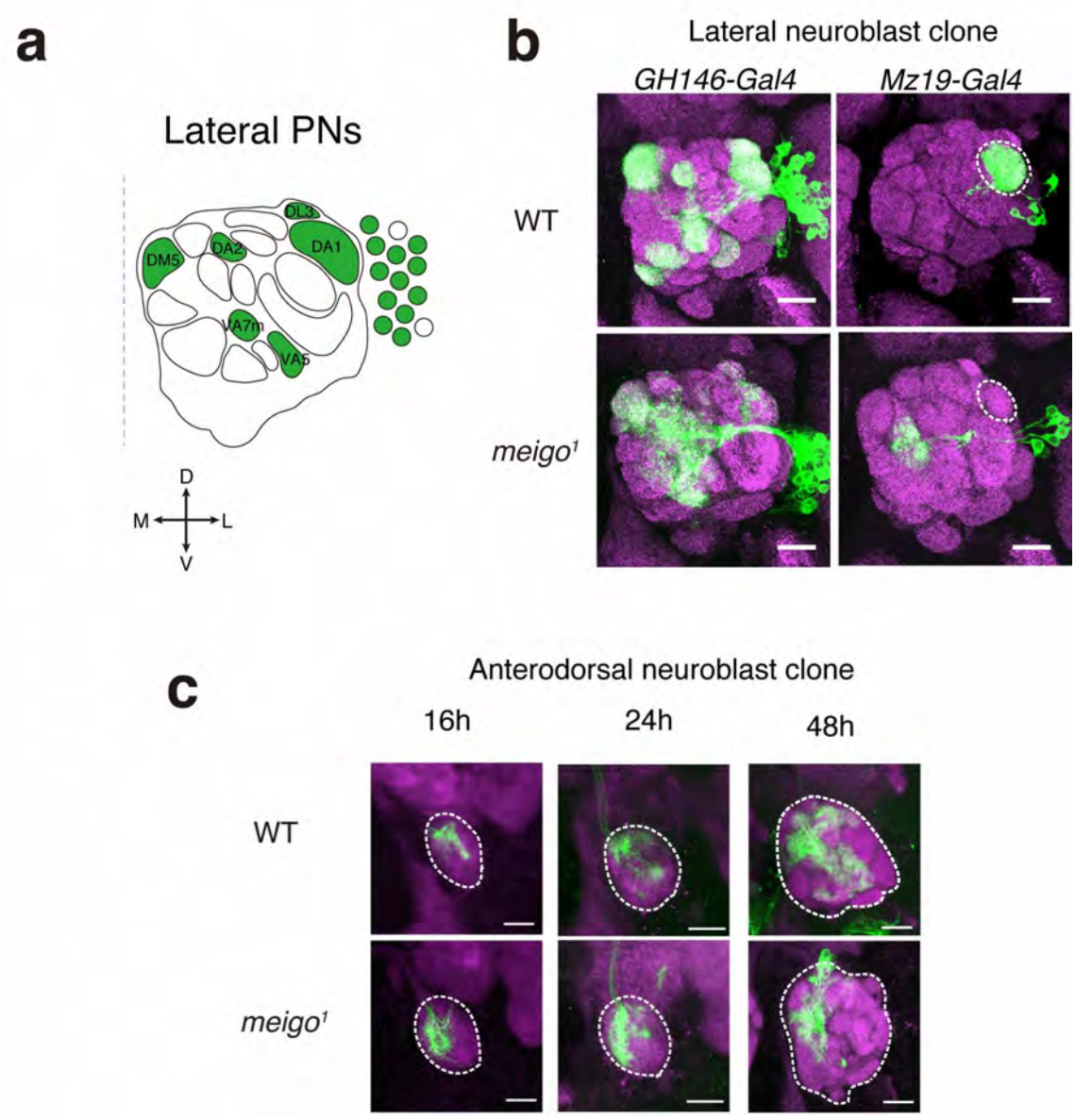

Supplementary Figure 1. Phenotype of *meigo*^{1} PN neuroblast clones

(**a**) Schematic of the MARCM PN neuroblast clones of lateral lineage labeled by *GH146-Gal4*. The target glomeruli of anterior surface of the antennal lobe are colored

in green. The name of each glomerulus is also indicated. (**b**) Lateral neuroblast MARCM clones labeled by *GH146-Gal4* or *Mz19-Gal4*. In the lateral lineage, as in the anterodorsal lineage, dendrite targeting of *meigo*^{1} PNs is shifted towards the medial side of the antennal lobe. Scale bar represents 20 μm. (**c**) Dendrites of MARCM PNs labeled by *GH146-Gal4* at 16, 24, and 48 hours after puparium formation (APF). The medial shift of dendrites is already seen at 16 hours APF, indicating that the initial targeting of dendrites is defective in *meigo*^{1} PNs. Green shows MARCM PNs and magenta shows *D*N-Cadherin (16 hours, 24 hours APF) or Brp (48 hours APF). The scale bar represents 20 μm.

Nature Neuroscience: doi:10.1038/nn.3389

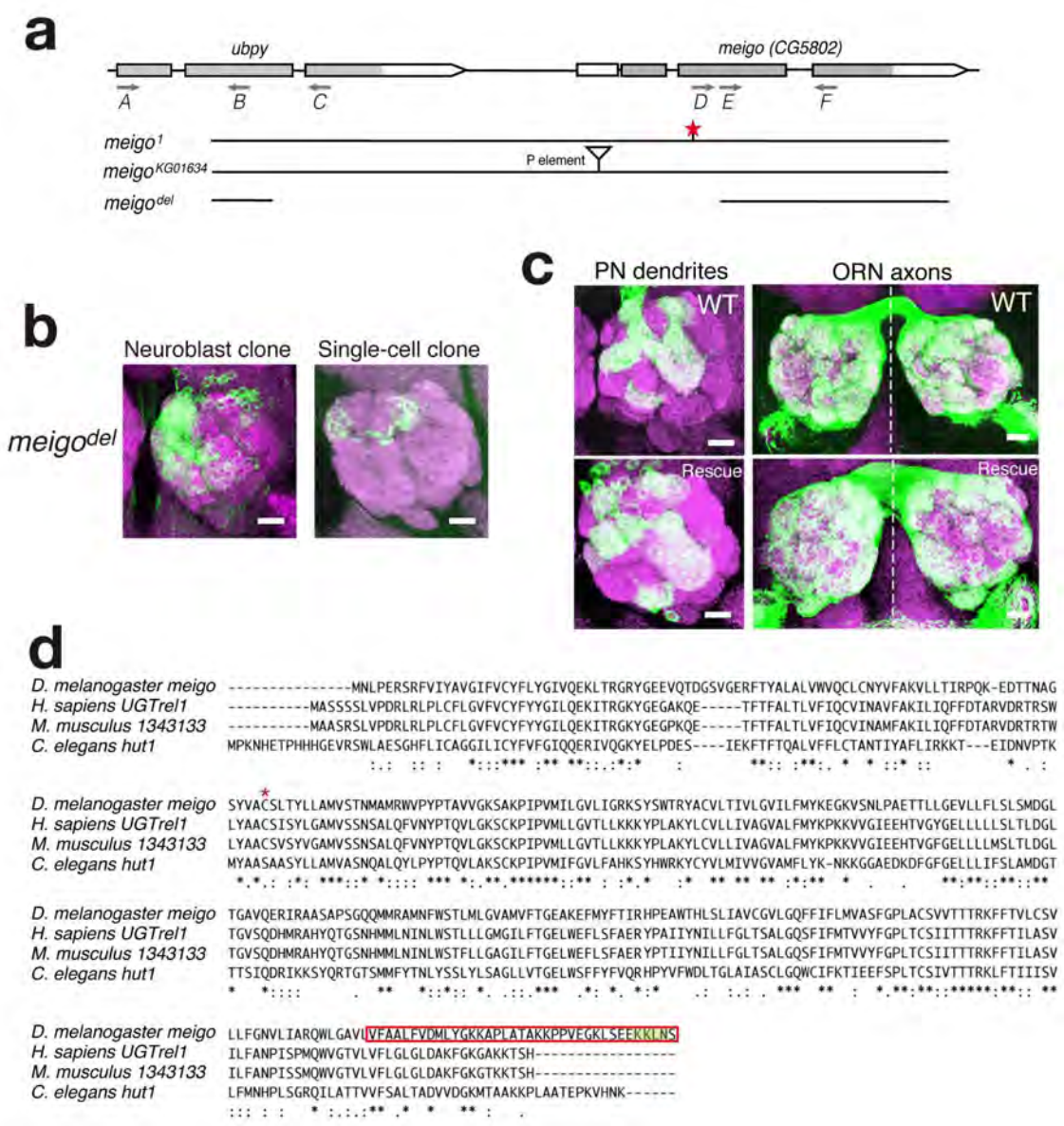

Supplementary Figure 2. ***meigo*** **functions in the PN and ORN cell-autonomously**

(**a**) Genomic organization of *CG5802* (*meigo*). The missense mutation, C89Y associated with the *meigo*^{1} allele is indicated by the red star. The deletion mutant *meigo*^{del} lacks about half of *meigo* and also a part of the neighboring gene *ubpy*. Primers used in genetic mapping are indicated with arrows and sequences are as follows (5'-3').

A: ACTGACTGGACTGAAGAATCTGGGC,

B: CGTGGCGGACTCCTTGTGGCAGGCC,

C: TCATGTACGAGCCAGAGTTACTGGG,

D: CCCATCCCCGTCATAGATCCTGGGCG,

E: AGGGCAAGGTGTCCAATTTGCCGGC,

F: GGTGAAGTACATGAATTCCTTGGCC.

The PCR using primer sets A/B or E/F resulted in amplification as wild type, while PCR using primer sets A/C or D/F failed to amplify any fragment. (**b**) PN MARCM clones homozygous for the *meigo*^{del} mutation. The medial shift of dendrites is clearly observed. Scale bar represents 20 μm. (**c**) MARCM rescue experiment. Expression of *meigo* cDNA restores normal dendrite targeting of *meigo*^{1} PN MARCM neuroblast clones and normal axon targeting of ORN *ey-flp FLP*-induced clones (compare with **Fig. 1** & **2**). White dotted line indicates midline. Scale bar represents 20 μm. (**d**) Alignment of the deduced amino acid sequences of Meigo and its homologs. Asterisks and colons indicate identical and similar residues, respectively. Meigo is predicted to have an ER retention sequence (KKXX; green box) at the C-terminus. A missense mutation (red star) is indicated at a conserved amino acid between the fly, mouse, and human orthologs. The antigen region for the anti-Meigo antibody is indicated by the red open box.

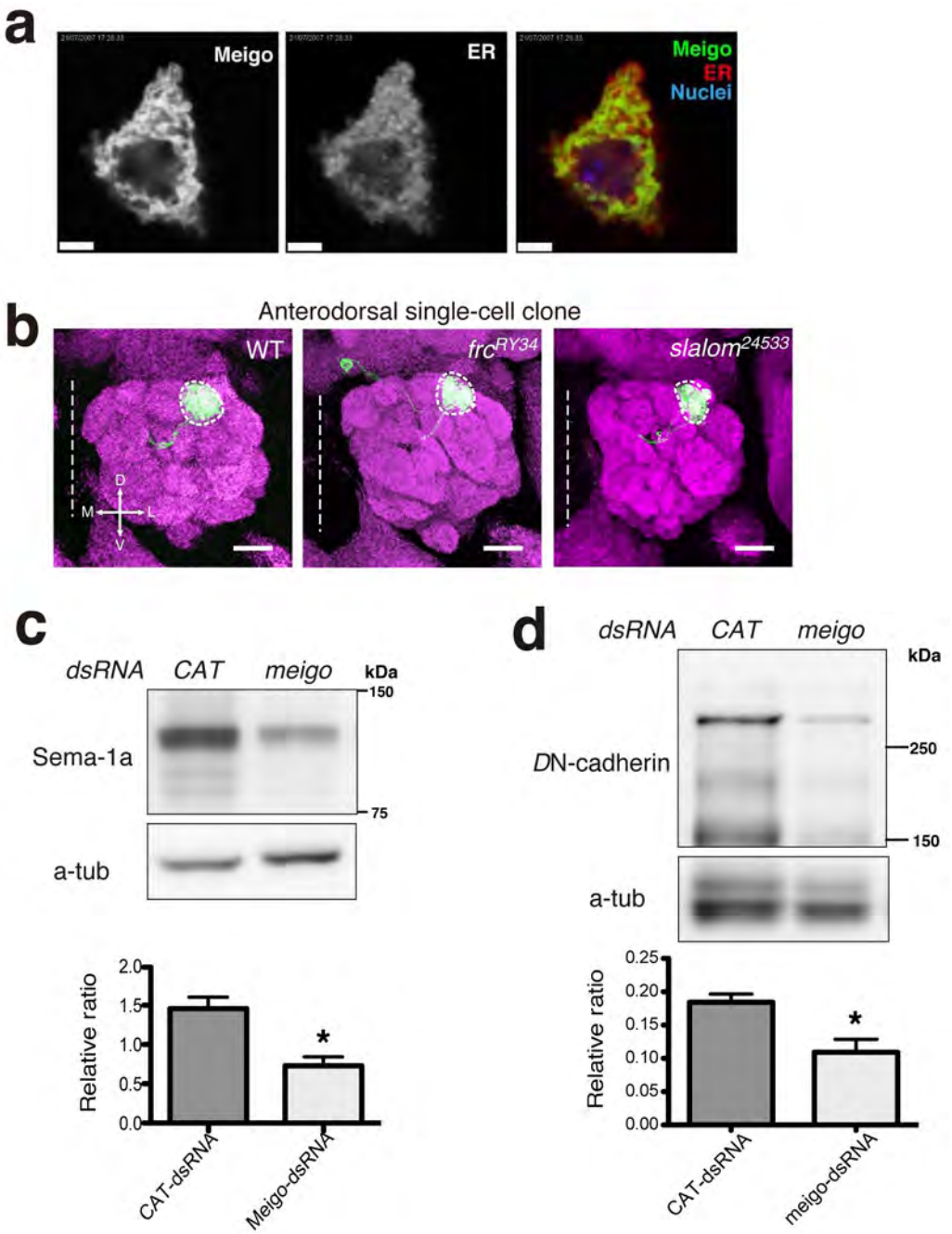

Supplementary Figure 3. Meigo is a unique ER protein that is required for expansion of ER folding capacity

(**a**) Immunohistochemistry of an S2 cell transiently transfected with *actin-Gal4* and *UAS-meigo*, stained with antibodies to Meigo (green), KDEL (red, an ER marker), and Hoechst (blue, nuclei). Scale bar represents 5 μm. (**b**) PN MARCM clones homozygous for mutations in other NSTs. *frc*^{RY34} mutant PNs or *slalom*^{24533} mutant

PNs did not exhibit any abnormal dendrite targeting. White dotted line indicates midline. Scale bar represents 20 μm. (**c**,**d**) The protein levels of transfected Semaphorin-1a (**c**, n=5) or *D*N-cadherin (**d**, n=3) in S2 cells were verified by Western blot. The anti-α-tubulin loading controls are below. Quantification of each protein normalized with α-tubulin revealed significant decrease in *meigo*-depleted cells compared to control. Mann Whitney test, $*P<0.05$.

Nature Neuroscience: doi:10.1038/nn.3389

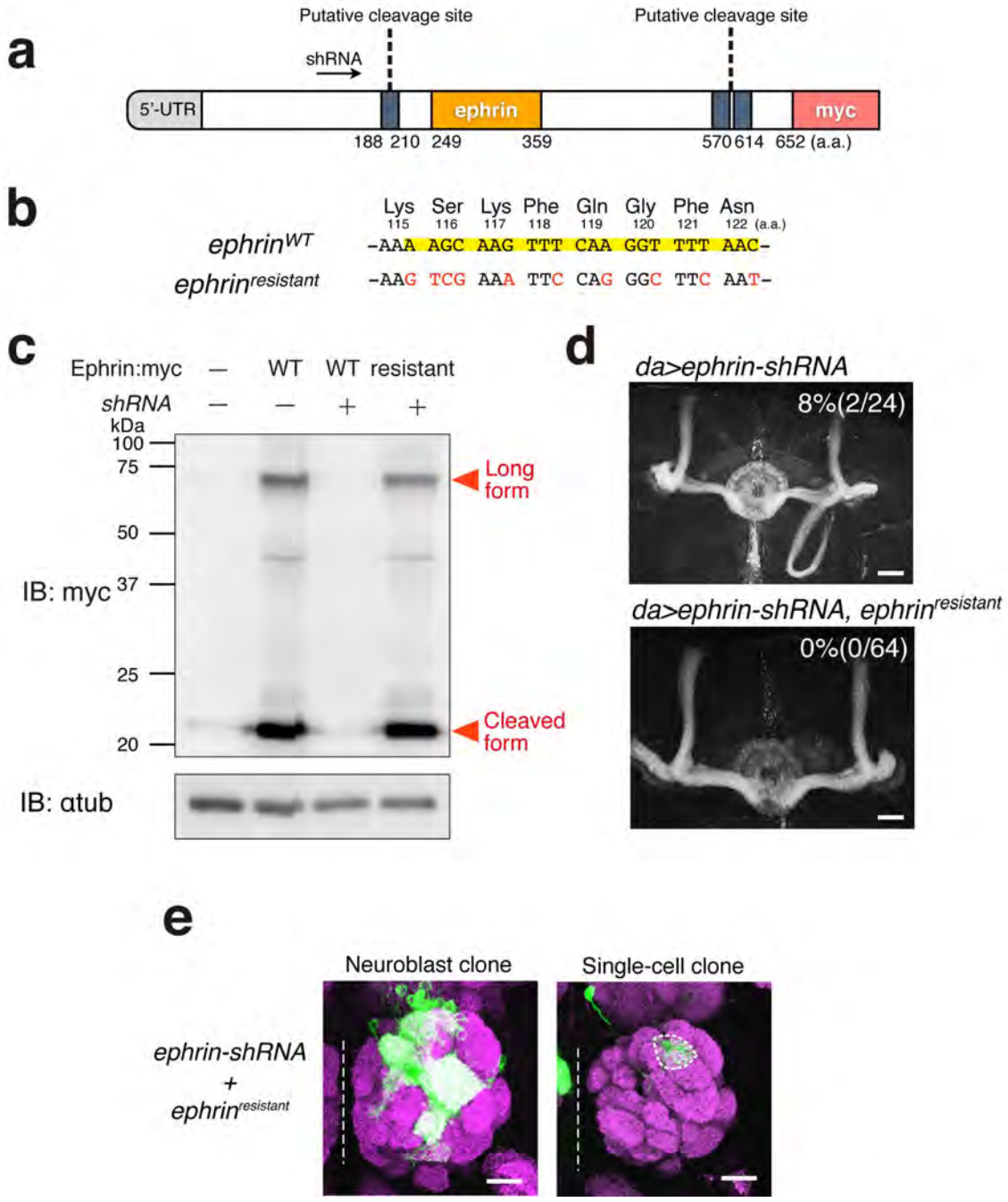

Supplementary Figure 4. Verification of *ephrin-shRNA*

(**a**) Gene structure of *ephrin-myc*. *Drosophila* Ephrin has a predicted Ephrin domain (orange) and three transmembrane regions (gray boxes). The C-terminal is tagged with 5x myc (pink box). Numbers indicate amino acid positions. The arrow indicates the target position for the *ephrin-shRNA*. The putative cleavage sites are indicated by dotted lines. (**b**) The 22 mer target sequence of *ephrin-shRNA* (yellow

box). In the *ephrin*^{resistant} construct, some nucleotides are changed without affecting the translational identity or efficiency (red letters). (**c**) Western blots with S2 cell lysates that were transiently transfected with *ephrin*^{WT}*-myc* or *ephrin*^{resistant}*-myc* together with *ephrin-shRNA*. The *ephrin-shRNA* is capable of reducing the protein level of Ephrin^{WT}-myc, but is not able to affect the level of Ephrin resistant form (Ephrin^{resistant}-myc). (**d**) The expression of *ephrin-shRNA* with a ubiquitous *Gal4* driver (*da-Gal4*) causes axon misguidance of mushroom body neurons (top row) detected by anti-FasII antibody, which is identical phenotype to the hypomorphic *ephrin* mutant. This axon guidance defect is rescued by co-expression of *ephrin*^{resistant}*-myc* (bottom row). Scale bar represents 20 μm. (**e**) The MARCM expression of *ephrin*^{resistant}*-myc* together with *ephrin-shRNA* expression using the *GH146-Gal4* driver, rescues the dendrite spillover in random directions. White dotted line indicates midline. Scale bar represents 20 μm.

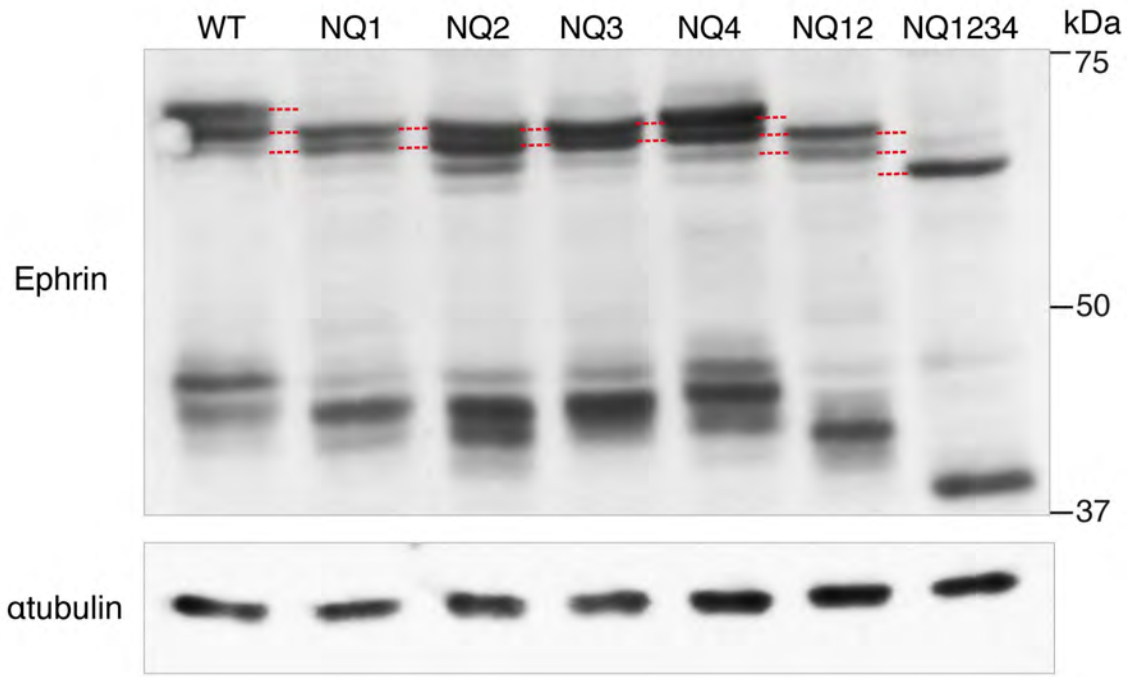

Supplementary Figure 5. Mutant form of Ephrin on *N*-glycosyltion sites

Immunoblot analyses of S2 cell lysates expressing various *N*-glycosylation mutant form of Ephrin-myc. The positions of mutated Asn are as follows. NQ1: Asn222, NQ2: Asn274, NQ3: Asn265, NQ4: Asn365, NQ12: Asn222 and Asn274, NQ1234: all of the four sites (Ephrin^{NQ}-myc in **Fig. 6b**).

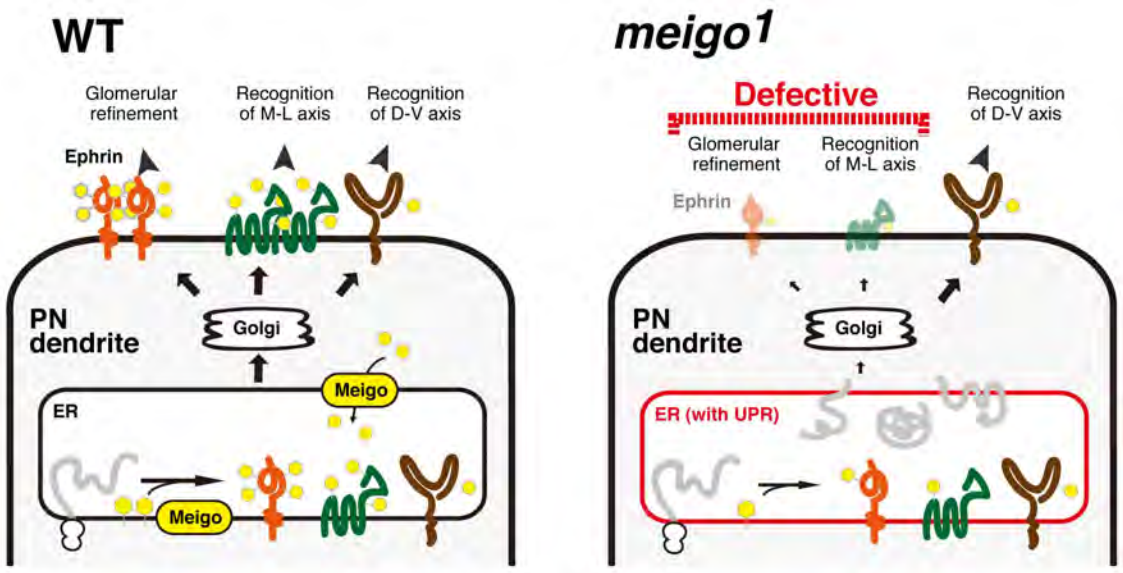

Supplementary Figure 6. Hypothetical model

In WT (left), Meigo is localized to the ER and functions in nucleotide sugar transport and/or *N*-glycosylation of nascent polypeptides. The various cell surface molecules are properly folded in the ER and are transported to the cell surface of dendrites, where they play a role in the glomerular refinement, mediolateral (M-L) targeting and/or dorsoventral (D-V) targeting of dendrites. For instance, Ephrin (orange protein) is properly *N*-glycosylated in the ER and functions in glomerular refinement. On the contrary, in *meigo*^{1} PNs (right), Meigo is absent from the ER, which results in less effective *N*-glycosylation and induction of the unfolded protein response (UPR). Based on our data (**Fig. 1c, d**), we hypothesize that susceptibility to *meigo* depletion might differ among cell surface molecules. Ephrin and cell surface molecules involved in M-L axis recognition (green protein) are preferentially affected while the molecules governing D-V axis recognition (brown protein) are unaffected. The yellow hexagon represents UDP-sugar or *N*-glycan.

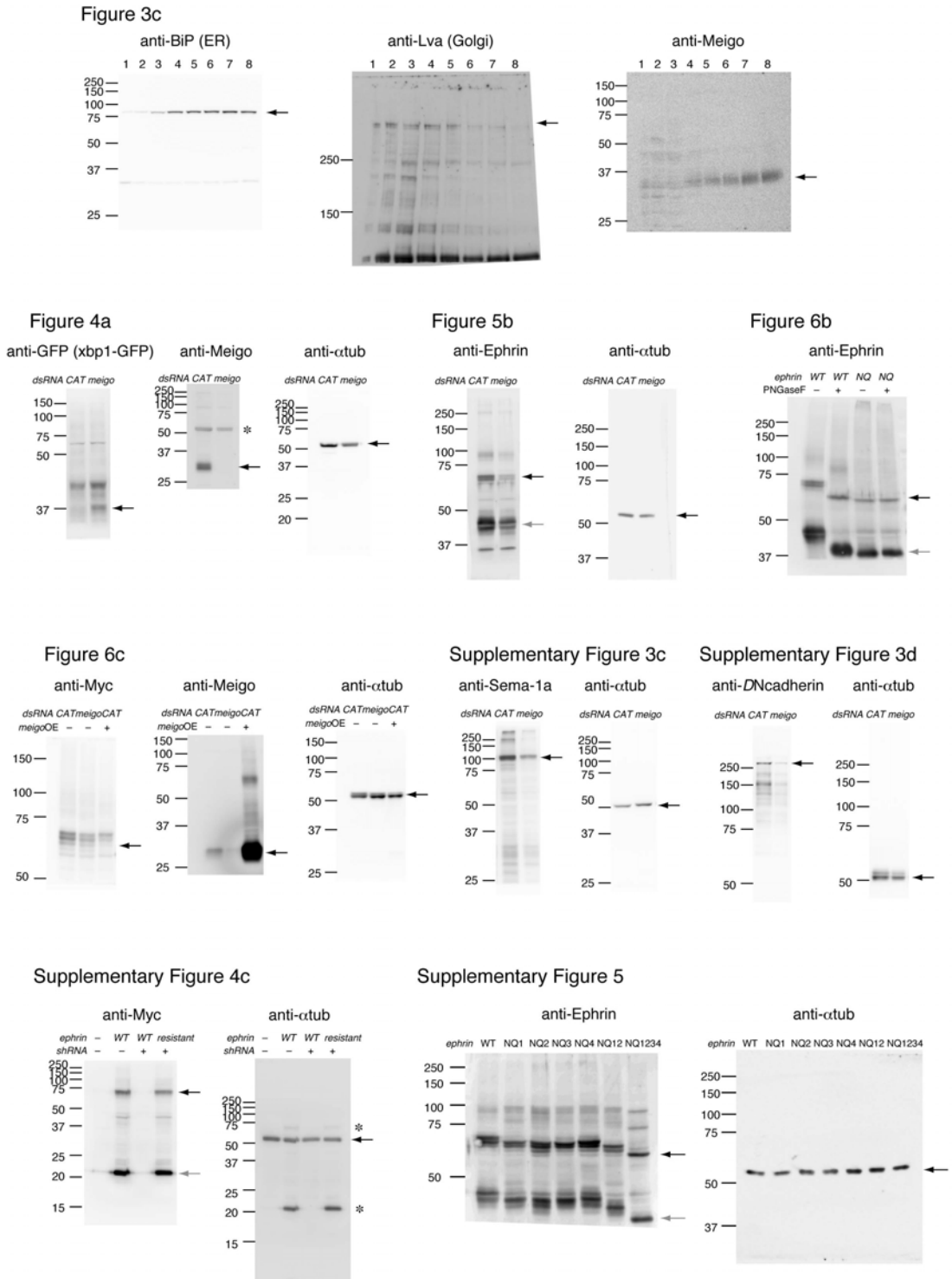

Supplementary Figure 7. Full-length pictures of western blots

Full-length pictures of the blots presented in **Fig. 3c, 4a, 5b, 6b, 6c, Supplementary Fig. 3c, 3d, 4c, and 5**. The black arrows indicate cropped region in the indicated figures. The gray arrows indicate cleaved form of Ephrin. Asterisks indicate the bands that were not completely stripped.

Function	Gene	Allele	*Mutant* (*shRNA*) phenotype of MARCM PN	Suppression of *meigo*^{1} PN by overexpressing each gene	Original papers
Nucleotide sugar transporter	*slalom*	*24533*	Normal	Not suppressed (5)	*EMBO J* **22**, 3635-3644 (2003)
	CG14511	*shRNA*	(Normal)	n.d.	
	Efr	*3*	Normal	Not suppressed (18)	*J Biol Chem* **285**, 4122-4129 (2010)
	Csat	*shRNA*	(Den/axon defective)	n.d.	
	CG14040	*shRNA*	(Den/axon defective)	n.d.	
	Gfr	–	n.d.	Not suppressed (14)	*Proc Natl Acad Sci U S A* **102**, 18532-18537 (2005)
	frc	*ry34*	Normal	Not suppressed (7)	*Proc Natl Acad Sci U S A* **102**, 13467-13472 (2005)
UDP-glucose:dolychyl-phospate	*wol*	*1, 2*	Normal	n.d.	*Development* **135**, 1745-1749 (2008)
Glycosyltransferase	*C1GalTA*	*2.1*	Normal	Not suppressed (6)	*Dev Dyn* **237**, 3703-3714 (2008)
	fdl	*P*	Cell lethal	n.d.	
	sfl	*l(3)03844*	Normal	n.d.	*Development* **126**, 3715-3723 (1999)
	DsiaT	*S23*	Spillover of dendrite	n.d.	*J Neurosci* **30**, 6466-6476 (2010)
HSPG	*ttv*	*524*	Axon misrouting (double mutant with botv)	n.d.	*Development* **131**, 73-82 (2004)
	botv	*510*	Normal	n.d.	*Development* **131**, 73-82 (2004)
	sotv	*326*	Normal	n.d.	*Development* **131**, 73-82 (2004)
	Hs6st	*d770*	Normal	n.d.	*J Cell Biol* **174**, 773-778 (2006)
Vesicle trafficking	*dar3(sar1)*	*11-3-63, P1*	Small AL	n.d.	*Cell* **130**, 717-729 (2007), *Dev Cell* **13**, 214-225 (2007)
	rab1	*e01287*	Cell lethal	n.d.	*Cell* **130**, 717-729 (2007)
	γCOP	*Δ114*	Normal	n.d.	*PLoS ONE* **3**, e1964 (2008)
ER stress related	*xbp1*	*K13803*	Normal	Not suppressed (4)	*EMBO J* **26**, 242-252 (2007)
	Ero1-like	*23T*	Spillover of dendrite	Not suppressed (17)	*J Cell Biol* **182**, 1113-1125 (2008)
	edem2	–	n.d.	Not suppressed (9)	*Proc Natl Acad Sci U S A* **106**, 17043-8 (2012)
Ceramide synthesis	*lace*	*K08,HG6*	Spillover of dendrite	n.d.	

Supplementary Table 1: Mutant analyses performed in this study

The function, gene name, and allele of tested candidate genes are listed. "The mutant phenotype of MARCM PNs" indicates the phenotypes of PN dendrite homozygous for

indicated mutant alleles. For the genes we were not able to get mutant, the phenotypes expressing *shRNA* for corresponding gene are indicated in parenthesis. However, further verification for the specificity of each *shRNA*s is required. "Suppression of *meigo*^{1} PN by overexpressing each gene" indicates the ability to suppress the mistargeting phenotypes observed in *meigo*^{1} PN single-cell clones. The numbers in the parenthesis indicate the observed number of single-cell clones. See **Supplementary Methods** for mutant alleles and transgenes used. n.d.: not determined.

Nature Neuroscience: doi:10.1038/nn.3389

Function	Gene	Allele	*Mutant* (*shRNA*) PN dendrite	Suppression of *meigo*^{1} phenotype by overexpressing each gene	Original papers
HSPG core protein	*dally*	*80*	Normal	n.d.	*Development* **131**, 601-611 (2004)
	dally-like protein	*A187*	Normal	n.d.	*Development* **131**, 601-611 (2004)
	syndecan	*Df48*	Normal	n.d.	*Curr Biol* **15**, 1701-1711 (2005)
	trol	*null*	Spillover	n.d.	*Dev Dyn* **224**, 403-412 (2002)
Cell surface protein	*Ncad*	-	Spillover*	Not suppressed	*Neuron* **42**, 63-75 (2004)
	Dscam	-	Reduced elaboration*	Not suppressed	*J Neurosci* **29**, 1904-1914 (2009)
	Sema1a	-	Ventromedial shift	Not suppressed	*Neuron* **20**, 207-220 (1998)
	Plexin	-	(Normal)	Not suppressed	*Neuron* **53**, 185-200 (2007)
	Robo	*Z3127, GA285*	Normal	n.d.	*Cell* **92**, 205-215 (1998)
	Robo2	*1*	Normal	Not suppressed	*Cell* **103**, 1033-1045 (2000)
	Robo3	*1*	Normal	Not suppressed	*Cell* **103**, 1033-1045 (2000)
	drl	*R343*	Normal	n.d.	*Nature* **422**, 583-588 (2003)
	Drl2	*E124*	Normal	n.d.	*Curr Biol* **17**, 1574-1579 (2007)
	dys	*Df(3R)6 184*	Normal	n.d.	*Dev Cell* **16**, 83-92 (2009)
	Eph	*shRNA*	(Spillover)	Not suppressed	*J Neurosci* **22**, 1338-1349 (2002)
	ephrin	*shRNA*	(Spillover)	Partially suppressed	*Development* **129**, 4205-4218 (2002), *Development* **133**, 1845-1854 (2006)
	VAP	*Δ44B*	Clogged dendrite	Not suppressed	*Neuron* **35**, 291-306 (2002), *Cell* **133**, 963-977 (2008)
Intracellular molecules contribute in Eph/Ephrin signal	*exn*	*EYΔ23*	Spillover (lateral lineage)	n.d.	*Neuron* **61**, 556-569 (2009)
	dock	*P1*	Over proliferation (lateral lineage)	n.d.	*Development* **130**, 1307-1316 (2003)
	pak	*16*	Normal	n.d.	*Cell* **101**, 283-294 (2000)

Supplementary Table 2: Search for the cell surface molecules that genetically interact with *meigo*

The function, gene name, and allele of tested candidate genes are listed. "The mutant phenotype of MARCM PNs" indicates the phenotypes of PN dendrite homozygous for indicated mutant alleles. For the genes we were not able to get mutant, the phenotypes expressing *shRNA* for corresponding gene are indicated in parenthesis. However, further verification for the specificity of each *shRNA*s is required. * indicate the

reported phenotypes in previous studies. "Suppression of *meigo*^{1} PN by overexpressing each gene" indicates the ability to suppress the mistargeting phenotypes observed in *meigo*^{1} PN single-cell clones. The numbers in the parenthesis indicate the observed number of single-cell clones. n.d.: not determined.

Nature Neuroscience: doi:10.1038/nn.3389

Nature Neuroscience: doi:10.1038/nn.3389

Supplementary Table 3. Genotype of each experiment

Figure		Genotype
Fig. 1c	WT (left to right)	*hs-FLP^{122} UAS-mCD8GFP/+; GH146-Gal4 UAS-mCD8GFP/+; FRT2A FRT82B y[+] /FRT82B tubP-Gal80*
		hs-FLP^{122} UAS-mCD8GFP/+;Mz19-Gal4 UAS-mCD8GFP/+; FRT2A FRT82B y[+]/FRT82B tubP-Gal80
		hs-FLP^{122} UAS-mCD8GFP/NP5103-Gal4; +/CyO; FRT2A FRT82B y[+]/FRT82B tubP-Gal80
	meigo^{1} (left to right)	*hs-FLP^{122} UAS-mCD8GFP/+; GH146-Gal4 UAS-mCD8GFP/+; FRT2A FRT82B meigo^{1} [y+]/ FRT82B tubP-Gal80*
		hs-FLP^{122} UAS-mCD8GFP/+;Mz19-Gal4 UAS-mCD8GFP/+; FRT2A FRT82B meigo^{1} [y+]/FRT82B tubP-Gal80
		hs-FLP^{122} UAS-mCD8GFP/NP5103-Gal4; +/CyO; FRT2A FRT82B meigo^{1} [y+]/FRT82B tubP-Gal80
Fig. 1e	WT	*hs-FLP^{122} UAS-mCD8GFP/+; GH146-Gal4 UAS-mCD8GFP/+; FRT2A FRT82B y[+]/FRT82B tubP-Gal80*
	meigo^{1}	*hs-FLP^{122} UAS-mCD8GFP/+; GH146-Gal4 UAS-mCD8GFP/+; FRT2A FRT82B meigo^{1} [y+]/FRT82B tubP-Gal80*
Fig.2a	WT	*ey-FLP UAS-mCD8GFP/pebbled-Gal4 UAS-mCD8GFP;; FRT2A FRT82B y[+] /FRT82B tubP-Gal80*
		ey-FLP UAS-mCD8GFP/+; Or88a-Gal4/+ ; FRT2A FRT82B y[+] /FRT82B tubP-Gal80
	meigo^{1}	*ey-FLP UAS-mCD8GFP/pebbled-Gal4 UAS-mCD8GFP;; FRT2A FRT82B meigo^{1} [y+]/FRT82B tubP-Gal80*
		ey-FLP UAS-mCD8GFP/+; Or88a-Gal4/+ ; FRT2A FRT82B meigo^{1} [y+] /FRT82B tubP-Gal80
Fig. 3e	*slalom*	*hs-FLP^{122} UAS-mCD8GFP/+; GH146-Gal4 UAS-mCD8GFP/ UAS-slalom; FRT2A FRT82B meigo^{1} [y+]/FRT82B tubP-Gal80*
	Efr	*hs-FLP^{122} UAS-mCD8GFP/+; GH146-Gal4 UAS-mCD8GFP/ UAS-Efr; FRT2A FRT82B meigo^{1} [y+]/FRT82B tubP-Gal80*
	frc	*hs-FLP^{122} UAS-mCD8GFP/+; GH146-Gal4 UAS-mCD8GFP/ UAS-frc-myc; FRT2A FRT82B meigo^{1} [y+]/FRT82B tubP-Gal80*
Fig.4c	WT	*hs-FLP^{122}; GH146-Gal4 UAS-mCD8RFP/ UAS-xbp1-EGFP; FRT2A FRT82B y[+]/FRT82B tubP-Gal80*
	meigo^{1}	*hs-FLP^{122}; GH146-Gal4 UAS-mCD8RFP/ UAS-xbp1-EGFP; FRT2A FRT82B meigo^{1} [y+]/FRT82B tubP-Gal80*
Fig. 4d	WT	*hs-FLP^{122} UAS-mCD8GFP/+; GH146-Gal4 UAS-mCD8GFP/+;FRT2A FRT82B y[+]/FRT82B tubP-Gal80*
	meigo^{1}	*hs-FLP^{122} UAS-mCD8GFP/+; GH146-Gal4 UAS-mCD8GFP/+; FRT2A FRT82B meigo^{1} [y+]/FRT82B tubP-Gal80*

Nature Neuroscience: doi:10.1038/nn.3389

Fig. 4e	(top to bottom)	*hs-FLP^{122} UAS-mCD8GFP/+; GH146-Gal4 UAS-mCD8GFP/+; FRT2A FRT82B y[+]/FRT82B tubP-Gal80*
		hs-FLP^{122} UAS-mCD8GFP/+; GH146-Gal4 UAS-mCD8GFP/UAS-Hsc3^{K97S}; FRT2A FRT82B y[+] /FRT82B tubP-Gal80
		hs-FLP^{122} UAS-mCD8GFP/+; GH146-Gal4 UAS-mCD8GFP/UAS-Hsc3^{D231S}; FRT2A FRT82B y[+] /FRT82B tubP-Gal80
		hs-FLP122 UAS-mCD8GFP/+; GH146-Gal4 UAS-mCD8GFP/UAS-ninaE^{G69D}; FRT2A FRT82B y[+] /FRT82B tubP-Gal80
		hs-FLP^{122} UAS-mCD8GFP/+; GH146-Gal4 UAS-mCD8GFP/+; FRT2A FRT82B meigo^{1} y[+]/FRT82B tubP-Gal80
		hs-FLP^{122} UAS-mCD8GFP/+; GH146-Gal4 UAS-mCD8GFP/UAS-Hsc3^{K97S}; FRT2A FRT82B meigo^{1} y[+] /FRT82B tubP-Gal80
		hs-FLP^{122} UAS-mCD8GFP/+; GH146-Gal4 UAS-mCD8GFP/UAS-Hsc3^{D231S}; FRT2A FRT82B meigo^{1} y[+] /FRT82B tubP-Gal80
		hs-FLP122 UAS-mCD8GFP/+; GH146-Gal4 UAS-mCD8GFP/UAS-ninaE^{G69D}; FRT2A FRT82B meigo^{1} y[+] /FRT82B tubP-Gal80
Fig. 5a	(top to bottom)	*hs-FLP^{122} UAS-mCD8GFP/+; GH146-Gal4 UAS-mCD8GFP/+; FRT2A FRT82B y[+]/FRT82B tubP-Gal80*
		hs-FLP^{122} UAS-mCD8GFP/+; GH146-Gal4 UAS-mCD8GFP/+; FRT2A FRT82B meigo^{1} y[+]/FRT82B tubP-Gal80
		hs-FLP^{122} UAS-mCD8GFP/+; GH146-Gal4 UAS-mCD8GFP/UAS-Dscam-GFP; FRT2A FRT82B meigo^{1} y[+]/FRT82B tubP-Gal80
		hs-FLP^{122} UAS-mCD8GFP/+; GH146-Gal4 UAS-mCD8GFP/UAS-sema1a FRT40A; FRT2A FRT82B meigo^{1} y[+]/FRT82B tubP-Gal80
		hs-FLP^{122} UAS-mCD8GFP/ UAS-DN-cadherin+; GH146-Gal4 UAS-mCD8GFP/+; FRT2A FRT82B meigo^{1} y[+]/FRT82B tubP-Gal80
		hs-FLP^{122} UAS-mCD8GFP/+; GH146-Gal4 UAS-mCD8GFP/UAS-ephrin; FRT2A FRT82B meigo^{1} y[+]/FRT82B tubP-Gal80
		hs-FLP^{122} UAS-mCD8GFP/+; GH146-Gal4 UAS-mCD8GFP/UAS-ephrin-myc; FRT2A FRT82B meigo^{1} y[+]/FRT82B tubP-Gal80
		hs-FLP^{122} UAS-mCD8GFP/+; GH146-Gal4 UAS-mCD8GFP/UAS-Eph-myc; FRT2A FRT82B meigo^{1} y[+]/FRT82B tubP-Gal80
Fig. 5d	WT	*hs-FLP^{122} UAS-mCD8GFP/+; GH146-Gal4 UAS-mCD8GFP/+; FRT2A FRT82B y[+] /FRT82B tubP-Gal80*
		hs-FLP^{122} UAS-mCD8GFP/NP5103-Gal4; +/CyO; FRT2A FRT82B y[+]/FRT82B tubP-Gal80
		hs-FLP^{122} UAS-mCD8GFP/+; GH146-Gal4 UAS-mCD8GFP/+; FRT2A FRT82B y[+] /FRT82B tubP-Gal80
	ephrin-shR	*hs-FLP^{122} UAS-mCD8GFP/+; GH146-Gal4 UAS-mCD8GFP/ UAS-ephrin-shRNA; FRT2A FRT82B y[+] /FRT82B tubP-Gal80*
		hs-FLP^{122} UAS-mCD8GFP/NP5103-Gal4; UAS-ephrin-shRNA/+; FRT2A FRT82B y[+]/FRT82B tubP-Gal80
		hs-FLP^{122} UAS-mCD8GFP/+; GH146-Gal4 UAS-mCD8GFP/ UAS-ephrin-shRNA; FRT2A FRT82B y[+] /FRT82B tubP-Gal80

Fig. 6e	(top to bottom)	*hs-FLP^{122} UAS-mCD8GFP/+; GH146-Gal4 UAS-mCD8GFP/+; FRT2A FRT82B y[+]/FRT82B tubP-Gal80*
		hs-FLP^{122} UAS-mCD8GFP/+; GH146-Gal4 UAS-mCD8GFP/+; FRT2A FRT82B meigo^{1} y[+]/FRT82B tubP-Gal80
		hs-FLP^{122} UAS-mCD8GFP/+; GH146-Gal4 UAS-mCD8GFP/UAS-ephrin-myc; FRT2A FRT82B meigo^{1} y[+]/FRT82B tubP-Gal80
		hs-FLP^{122} UAS-mCD8GFP/+; GH146-Gal4 UAS-mCD8GFP/UAS-ephrin^{NQ}-myc; FRT2A FRT82B meigo^{1} y[+]/FRT82B tubP-Gal80
Fig. S1b	WT (left to right)	*hs-FLP^{122} UAS-mCD8GFP/+;GH146-Gal4 UAS-mCD8GFP/+; FRT2A FRT82B y[+]/FRT82B tubP-Gal80*
		hs-FLP^{122} UAS-mCD8GFP/+;Mz19-Gal4 UAS-mCD8GFP/+; FRT2A FRT82B y[+]/FRT82B tubP-Gal80
	meigo^{1} (left to right)	*hs-FLP^{122} UAS-mCD8GFP/+; GH146-Gal4 UAS-mCD8GFP/+;FRT2A FRT82B meigo^{1} y[+]/FRT82B tubP-Gal80*
		hs-FLP^{122} UAS-mCD8GFP/+;Mz19-Gal4 UAS-mCD8GFP/+; FRT2A FRT82B meigo^{1} y[+]/FRT82B tubP-Gal80
Fig. S1c	WT	*hs-FLP^{122} UAS-mCD8GFP/+;GH146-Gal4 UAS-mCD8GFP/+; FRT2A FRT82B y[+]/FRT82B tubP-Gal80*
	meigo^{1}	*hs-FLP^{122} UAS-mCD8GFP/+; GH146-Gal4 UAS-mCD8GFP/+;FRT2A FRT82B meigo^{1} y[+]/FRT82B tubP-Gal80*
Fig. S2b	*meigo^{del}*	*hs-FLP^{122} UAS-mCD8GFP/+; GH146-Gal4 UAS-mCD8GFP/+; FRT2A FRT82B meigo^{del} y[+]/ FRT82B tubP-Gal80*
Fig. S2c	(PN Rescue)	*hs-FLP^{122} UAS-mCD8GFP/+; GH146-Gal4 UAS-mCD8GFP/UAS-meigo; FRT2A FRT82B meigo^{1} y[+]/FRT82B tubP-Gal80*
	(ORN Rescue)	*ey-FLP UAS-mCD8GFP/pebbled-Gal4 UAS-mCD8GFP;UAS-meigo/+; FRT2A FRT82B meigo^{1} y[+]/FRT82B tubP-Gal80*
Fig. S3b	*frc^{RY34}*	*hs-FLP^{122} UAS-mCD8GFP/+; GH146-Gal4 UAS-mCD8GFP/+; frc^{RY34} FRT2A/tubP-Gal80 FRT2A*
	slalom^{24533}	*hs-FLP^{122} UAS-mCD8GFP/+; GH146-Gal4 UAS-mCD8GFP/+;slalom^{24533} FRT2A/tubP-Gal80 FRT2A*
Fig. S4d		*UAS-ephrin-shRNA/+; daughterless-Gal4/+*
	(Rescue)	*UAS-ephrin-shRNA/+; daughterless-Gal4/UAS-ephrin^{resistant}*
Fig. S5e	(Rescue)	*hs-FLP^{122} UAS-mCD8GFP/+; UAS-ephrin-shRNA FRT40A/tubP-Gal80 FRT40A GH146-Gal4; UAS-ephrin^{Resistant}/+*